5-2011

Discharge Coefficient Performance of Venturi, Standard Concentric Orifice Plate, V-Cone, and Wedge Flow Meters at Small Reynolds Numbers

Colter L. Hollingshead
Utah State University

DISCHARGE COEFFICIENT PERFORMANCE OF VENTURI, STANDARD CONCENTERIC ORFICE PLATE, V-CONE, AND WEDGE FLOW METERS AT SMALL REYNOLDS NUMBERS

by

Colter L. Hollingshead

A thesis submitted in partial fulfillment
of the requirements for the degree

of

MASTER OF SCIENCE

in

Civil and Environmental Engineering

Approved:

_____	_____
Michael C. Johnson Major Professor	Steven L. Barfuss Committee Member
_____	_____
Robert E. Spall Committee Member	Byron R. Burnham Dean of Graduate Studies

UTAH STATE UNIVERSITY
Logan, Utah

2011

ABSTRACT

Discharge Coefficient Performance of Venturi, Standard Concentric Orifice Plate, V-Cone, and Wedge Flow Meters at Small Reynolds Numbers

by

Colter L. Hollingshead, Master of Science

Utah State University, 2011

Major Professor: Dr. Michael C. Johnson
Department: Civil and Environmental Engineering

The relationship between the Reynolds number (Re) and discharge coefficients (C) was investigated through differential pressure flow meters. The focus of the study was directed toward very small Reynolds numbers commonly associated with pipeline transportation of viscous fluids. There is currently a relatively small amount of research that has been performed in this area for the Venturi, standard orifice plate, V-cone, and wedge flow meters. The Computational Fluid Dynamics (CFD) program FLUENT© was used to perform the research, while GAMBIT© was used as the preprocessing tool for the flow meter models created. Heavy oil and water were used separately as the two flowing fluids to obtain a wide range of Reynolds numbers with high precision. Multiple models were used with varying characteristics, such as pipe size and meter geometry, to obtain a better understanding of the C vs. Re relationship. All of the simulated numerical models were compared to physical data to determine the accuracy of the models. The study indicates that the various discharge coefficients decrease rapidly as the Reynolds number

approaches 1 for each of the flow meters; however, the Reynolds number range in which the discharge coefficients were constant varied with meter design. The standard orifice plate does not follow the general trend in the discharge coefficient curve that the other flow meters do; instead as the Re decreases, the C value increases to a maximum before sharply dropping off. Several graphs demonstrating the varying relationships and outcomes are presented. The primary focus of this research was to obtain further understanding of discharge coefficient performance versus Reynolds number for differential producing flow meters at very small Reynolds numbers.

(93 pages)

ACKNOWLEDGMENTS

This project would not have been complete without the support of many people. The financial support that has been provided by the Utah Water Research Laboratory is greatly appreciated. I would like to thank my major professor, Dr. Michael Johnson, for giving me the opportunity to perform research at the UWRL and explore the world of hydraulics first hand. I would especially like to thank my additional committee members, Steven Barfuss and Dr. Robert Spall, for their assistance throughout the completion of my thesis and for their willingness to help with any problems.

I would also like to thank Ryan Christensen for CFD assistance and Marshall Bailey for additional McCrometer V-cone meter information. Special thanks also to The High Performance Computing Center at Utah State University for allowing me to run all of my models on one of the available clusters.

I would finally like to give special thanks to all my family and friends who have given me support throughout the past year, because without them none of this would be possible.

Colter L. Hollingshead

CONTENTS

LIST OF TABLES

LIST OF FIGURES

NOTATIONS

A = area of Pipe

A_0 = turbulence model constant

C = discharge coefficient

CFD = Computational Fluid Dynamics

$C_{1\varepsilon}$ = model constant

$C_{2\varepsilon}$ = model constant

$C_{3\varepsilon}$ = model constant

cfs = cubic feet per second

cms = cubic meters per second

cP = Centipoise

cm = centimeters

D = Pipe diameter

d = Flow meter object diameter

DS = Downstream

ft = feet

g = acceleration of gravity

gpm = gallons per minute

H = Wedge segment height

H/D = Wedge apex height/Pipe Diameter

h_w = Differential head

k = Turbulent kinetic energy

lps = Liters per second

m = meters

N = Dimensional constant

N-S = Navier-Stokes Equations

$P_{\square}$ = Production of buoyancy term

p = static pressure

Q, q = mass flow rate

Re = Reynolds Number

s = seconds

t = time

US = Upstream

u = component of velocity in x direction

V = Average velocity

v = component of velocity in y direction

w = component of velocity in z direction

x = horizontal cross section direction

y = vertical cross section direction

z = pipe axial direction

β = Relationship between pipe diameter and object diameter

ϒ = specific weight of fluid

δ = Kronecker delta function

$\square$ = Dissipation rate

μ = dynamic viscosity of fluid

υ = kinematic viscosity of fluid

π = pi term

ρ = density of fluid

$\sigma_{\square}$ = Prandtl number for □

σ_k = Prandtl number for k

τ = Stress tensor

φ = Cell center value

Ω = Mean rate of tensor rotation

ω_k = Angular velocity

CHAPTER I

INTRODUCTION

In response to there being an increased need for accurate flow measurements of viscous fluids through various types of differential pressure flow meters, computer simulations were conducted as part of this research to more accurately define the characteristics of the discharge coefficient, (C) at small Reynolds numbers. The heavy oil industry has found that with rising oil prices it has become more economical for companies to pursue the extraction of extremely viscous oils, which results in small Reynolds numbers flowing through the pipe and consequently the meters (GOA, 2009). Accurate flow measurement is one of the greatest concerns among many industries, because uncertainties in product flows can cost companies considerable profits. Currently there is little known about the C values at small Reynolds (Re) numbers for the meters in this report (Miller, 1996), since calibrations for these meters are generally performed in a laboratory using cold water. Differential pressure meters are popular for these applications because they are relatively inexpensive and produce reliable results.

Four different types of differential pressure flow meters were studied which include: Venturi, standard concentric orifice plate, V-cone, and wedge flow meters shown in Fig. 1. The Venturi flow meter obtains a pressure differential by constricting the flow area and therefore increasing the velocity at the constriction, which creates a lower pressure according to Bernoulli's Theorem. The concentric orifice plate flow meter reduces the pressure by forcing the fluid through a thin plated circular opening smaller than the pipe diameter. The V-cone flow meter has a cone shaped obstruction in the middle the pipe, which forces the flow around the outside of the cone creating a

pressure differential. The wedge flow meter has a wedge shaped obstruction located in the upper portion of the pipe, which reduces pressure on the downstream side of the wedge. Fig. 1 shows sketches of the different types of meters investigated.

The viscosity of a fluid is inversely proportional to the Reynolds number for a specific flow, so increasing the viscosity of the fluid results in a smaller Reynolds number for a viscous fluid. With an increased accuracy in numerical modeling over the years, it is now plausible to use it for flow conditions where experimental procedures may be inadequate. Viscous fluids with very small Reynolds numbers cannot accurately be tested in the laboratory with water because the pressure differences are too small to accurately measure. Therefore, computer modeling simulations can be used to characterize the discharge coefficients over very small Reynolds numbers. All of the computer model simulations were verified by comparing them to lab data or previous findings where the discharge coefficients were well known. Once the numerical models were verified they were taken to more viscous regions where experimental data with water would have a high degree of uncertainty.

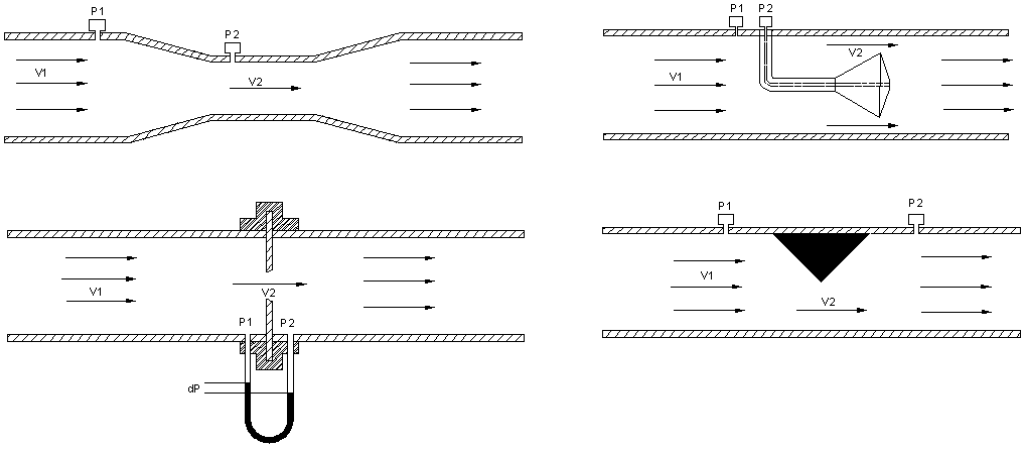

Fig. 1. Sketches of the investigated flow meters.

Reynolds numbers deserve excessive observation when it comes to analyzing the capabilities of flow meters. The value of Re for a particular pipe flow can be decreased by either decreasing velocity, or increasing the fluids viscosity. As the viscosity of a fluid increases in a pipeline, the consequent wall shear rate decreases resulting in a more uniform flow profile (Clark, 1993). Therefore, to obtain accurate CFD data for extremely small Re it was necessary to increase the viscosity of the flowing fluid which for this study was a realistic heavy oil crude viscosity of 200 centipoise (Ashrafizadeh and Kamran, 2010).

The primary objectives of this thesis were as follows:

1) Evaluate the possibility of a numerical computer solution by comparing numerical results to actual laboratory data.
2) Perform an extensive amount of simulation on the different models being analyzed.
3) Provide guidelines for the use of these flow meters at small Re numbers.
4) Provide a wide range of discharge coefficients characteristics for these four types of differential producing flow meters.

The paper will commence by presenting previous literature knowledge on the subject and what is currently available in practice. The theoretical background of FLUENT© and flow meter equations will then be presented. This will be followed by the process used for setting up the simulations and a procedure to enable the prediction of the discharge coefficients for the flow meters. The actual numerical procedure will then be fully described along with the corresponding model results. Finally the findings from the

results will be summarized and presented to demonstrate their beneficial uses to the flow meter industry.

CHAPTER II

LITERATURE REVIEW

A substantial amount of research has been done concerning the discharge coefficients of flow meters, but very little of it has dealt with extremely small Reynolds numbers. Depending on a fluids viscosity the definition of small and large Reynolds numbers can vary. For water, small Reynolds numbers can be defined as Re < 10,000, while large Reynolds numbers are Re > 1,000,000 (Miller, 1996).

Miller, Pinguet, Theuveny, and Mosknes conducted a study to evaluate the effects of an emulsion mixture through a Venturi flow meter (Miller et al., 2009). The primary focus of the study was to determine heavy oil fluid flows with viscosities ranging from 3-300 centipoise (cP). The testing performed consisted of an emulsion mixture flow loop, where the mixture was pumped through the system at different velocities to determine the effect of viscosity on the discharge coefficient. Reynolds numbers ranged from 400 to 24,000 in the study, and the researchers concluded that the following Eq. 1 could be used to estimate the discharge coefficient for different ranges of Reynolds numbers.

$$Cd = B + A * \log(Re) \quad (1)$$

Even though this equation can be used to estimate the discharge coefficient and consequently the flow through a Venturi flow meter, there is still significant uncertainty with the values of A and B depending on the viscosity of the fluid being used. Miller et al. (2009) were able to determine that the resulting relative errors for Re > 2000, ranged from 2 to 4 %, while the uncertainty grew for values from 400 < Re < 2000 to as much as 6 %.

Britton and Stark conducted experiments to determine discharge coefficients for sharp edged orifice plates which are hydraulically similar to the standard orifice plate (Britton and Stark, 1986). Their research consisted of the comparison between the sharp edge and quadrant edge orifice plates with beta ratios (ratio of throat diameter to inlet diameter) of 0.25, 0.39, and 0.51 with upstream pipe diameters being 3.055 or 4.032 inches. The testing was performed using an oil flow test facility at the Colorado Engineering Experiment Station Inc. (CEESI). Reynolds numbers in the experiment ranged from 1,000 – 50,000 with the corresponding discharge coefficients varying from 0.605 - 0.695 for the sharp edged orifice plate. It was found that as the beta ratio increased to the upper value of 0.51, so too did the variance of the discharge coefficient over the experimental range. It was proposed by the researches that the reasoning for a hump like formation at Reynolds numbers less than 3,000 was due to laminar parabolic flow, which had less restriction from an orifice plate unlike turbulent flow where discharge coefficients were much smaller as seen in Fig. 2.

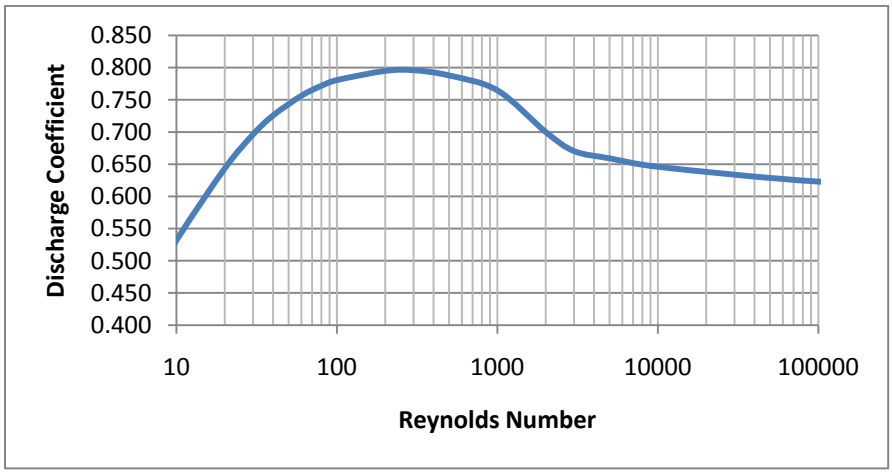

Fig. 2. Typical orifice plate re vs. C relationship.

Singh et al. (2006) studied the discharge coefficients of the V-Cone flow meter through multiple laboratory runs. The group's experimental setup for the system procedure included: water supplied by an over head water tank, an isolating valve 60 diameters upstream, a disturbance valve of varying distances upstream, the V-cone flow meter, a downstream flow control valve over 20 diameters away, and an outflow weight tank. The pipe diameter utilized was 2.047 inches, and the two different beta ratios used were 0.64 and 0.77. Oil, water, and a mixture of the two were run through the experimental setup to determine the effects that a viscous fluid may have on the behavior of the V-cone. Singh et al. proposed that for Reynolds numbers between 1,250 and 254,000 that the average discharge coefficient for the beta values of 0.64 and 0.77 were 0.7256 and 0.7310, respectively. It was concluded that disturbances greater than 10 diameters upstream of the V-cone had little effect on the resulting coefficient, as the geometry of the V-cone was able to reshape the velocity profile before the upstream pressure tap location. Their study indicated that the discharge coefficient and Reynolds number are nearly independent of each other over the ranges tested. In addition it was suggested that the discharge coefficient has very little dependence on the beta value.

Tan et al. (2009) described the results of work completed for two-phase flow measurements using a V-cone flow meter. An oil and water mixture was used in a 2-in diameter pipe with a V-cone beta ratio of 0.65. The experiments were conducted in a test loop at Tianjin University of China. For this study the oil and water were pumped separately into the system and thoroughly mixed at the entrance nozzle, then ran through the V-cone, into a separation tank, and finally returning to their designated tanks as the process was repeated for each of the tests. After the tests were completed, it was found

that runs with Reynolds numbers between 25,000 and 85,000 had a discharge coefficient ranging from 0.8 to 0.85 with an average value of 0.83. They proposed that the separated model that follows was more accurate than the homogenous mixture model for calculating mass flow rate of an oil-water mixture.

$$W_m = \frac{CA\sqrt{2\Delta P_{TP}\rho_2}}{\sqrt{1-\beta^4\left[x+(1-x)\sqrt{\frac{\rho 2}{\rho 1}}\right]}} \quad (2)$$

This model is important because these types of mixtures are often used in the oil industry to transport viscous heavy oil efficiently.

Banchhor et al. (2002) explored the effects of vertex angles and the apex height/diameter ratio (H/D) on the discharge coefficient of wedge flow meters using CFD. Their experiment was conducted using FLUENT© with the application of the SIMPLE pressure algorithm and the k-epsilon turbulence model. The simulations consisted of varying wedge flow meters placed in the center of a 20-inch long pipe with a 2-inch diameter. Vertex angles of 60 and 90 degrees were used along with different vertex radii. It was found that as the radii were increased from 0 to 6 mm the resultant C value also increased. When comparing the Re vs. C, it was found that the C remained fairly constant for much of the Re range tested. It was also proposed from the results that as the H/D value increased so too did the average discharge coefficient.

Yoon and colleagues' (2007) study resulted in a proposed discharge coefficient equation for segmental wedge flow meters. The experiment was a closed loop system consisting of the following elements: a reservoir tank, upstream calibrated magnetic flow meter, a wedge flow meter, differential pressure and temperature monitors up and downstream, a collection chamber, and pump to circulate the water. Five different beta

values were studied in the project which varied from 0.3 to 0.7. The results of the study concluded that for each beta value the discharge coefficient remained constant over a wide range of Re numbers. The five different beta ratios had varying C's, but they formulated the following equation to predict the discharge coefficients for H/D (Z) values between 0.3 and 0.7.

$$C_d = 0.9136Z^{0.1303} - 23.363Z^4 + 50.378Z^3 - 37.246Z^2 + 11.062Z - 1.1055 \quad (3)$$

CHAPTER III

DISCHARGE COEFFICIENTS AT SMALL REYNOLDS NUMBERS THROUGH DIFFERNTIAL PRODUCING FLOW METERS

Theoretical background

Governing equations that describe as well as possible the physical phenomena occurring are the primary building blocks used in numerical analysis. When using FLUENT© there are many different equation options for the user to choose from, but the primary equations used to describe the motion of fluids are the Navier-Stokes (N-S) equations. It is important to note that for the N-S equations to be valid for the models simulated in this research, that the flows contained only incompressible Newtonian fluids. These particular equations which are solved simultaneously include; directional momentum equations, the continuity equation and the energy equation with some variations depending on the type of problem being solved. For incompressible flows, as in the present study, the energy equation does not need to be solved simultaneously with momentum and continuity. The continuity equation otherwise known as the conservation of mass can be written as (NASA, 2008)

$$\frac{\partial(\rho u)}{\partial x} + \frac{\partial(\rho v)}{\partial y} + \frac{\partial(\rho w)}{\partial z} = 0 \quad (4)$$

where ρ = density of fluid being used, kg/m^3

x, y, z = coordinates in three dimensions, m

u, v, w = velocity components in x, y and z directions respectively, m/s^1

The momentum equations are as follows for the three dimensional models (NASA, 2008)

$$\frac{\partial(\rho u^2)}{\partial x}+\frac{\partial(\rho uv)}{\partial y}+\frac{\partial(\rho uw)}{\partial z}=-\frac{\partial p}{\partial x}+\frac{1}{Re_r}\left(\frac{\partial \tau_{xx}}{\partial x}+\frac{\partial \tau_{xy}}{\partial y}+\frac{\partial \tau_{xz}}{\partial z}\right) \quad (5)$$

$$\frac{\partial(\rho uv)}{\partial x}+\frac{\partial(\rho u^2)}{\partial y}+\frac{\partial(\rho vw)}{\partial z}=-\frac{\partial p}{\partial y}+\frac{1}{Re_r}\left(\frac{\partial \tau_{xy}}{\partial x}+\frac{\partial \tau_{yy}}{\partial y}+\frac{\partial \tau_{yz}}{\partial z}\right) \quad (6)$$

$$\frac{\partial(\rho uw)}{\partial x}+\frac{\partial(\rho vw)}{\partial y}+\frac{\partial(\rho w^2)}{\partial z}=-\frac{\partial p}{\partial z}+\frac{1}{Re_r}\left(\frac{\partial \tau_{xz}}{\partial x}+\frac{\partial \tau_{yz}}{\partial y}+\frac{\partial \tau_{zz}}{\partial z}\right) \quad (7)$$

where p = the static pressure at a computational grid point, N/m^2

t = time in seconds

$s\tau$ = stress tensor of the fluid, N/m^2

The shear tensor equation is given by

$$\tau=\left[\mu\left(\frac{\partial u_i}{\partial x_j}+\frac{\partial u_j}{\partial x_i}\right)\right]-\frac{2}{3}\mu\frac{\partial u_i}{\partial x_i}\delta_{ij} \quad (8)$$

where μ = the effective dynamic viscosity of fluid in Ns/m^2

δ_{ij} = Kronecker delta function used for volume fluctuations

Newton's second law states that the rate of change in momentum determines the sum of forces on a fluid particle (Versteeg and Malalasekera, 2007). The momentum equations described are used in FLUENT© to determine the motion of the fluid in the 3 dimensions being analyzed. Once the forces on each of the computational points are found, the resultant vector can then be produced along with results of the continuity equation.

The second order upwind scheme shown in eq. 9 was used to increase model accuracy (Fluent Inc., 2006). The method uses an expanded Taylor series expansion of a cell centered solution about the cell centroid (Fluent Inc., 2003).

$$\emptyset_{f,SOU}=\emptyset+\nabla\emptyset*\underset{r_v}{\rightarrow} \quad (9)$$

where $\emptyset$ = is the cell centered value

$\nabla\emptyset$ = the value of the gradient in the upstream cell

$\underset{r_v}{\rightarrow}$ = the displacement vector from upstream cell centroid to the face centroid

The value of the gradient upstream $\nabla\emptyset$ is computed using the following

$$\nabla\emptyset = \frac{1}{V} * \sum_{f}^{N_{faces}} \emptyset_f * \underset{A}{\rightarrow} \quad (10)$$

where $\emptyset_f$ = the face values

$\underset{A}{\rightarrow}$ = face area

V = cell volume

Turbulence creates energy losses and fluctuations in the flow that need to be calculated to obtain a more accurate solution. The realizable k-epsilon model was found to be the most accurate for modeling turbulent flows for the flow meters, because its results were most comparable to the laboratory data. Eqs. 11 and 12 are the kinetic energy (k) and dissipation rate (□) transportation equations, which were solved simultaneously to determine velocities throughout the turbulent model (Versteeg and Malalasekera, 2007).

$$\frac{\partial}{\partial t}(\rho K) + div(\rho K U) = div\left[\frac{\mu_t}{\sigma_k}\, grad\, k\right] + 2\mu S_{ij} * S_{ij} - \rho\varepsilon \quad (11)$$

and

$$\frac{\partial}{\partial_t}(\rho\epsilon) + div(\rho\varepsilon U) = div\left[\frac{\mu_t}{\sigma_\epsilon}\, grad\, \epsilon\right] + C_{1\epsilon}\frac{\epsilon}{k} * 2\mu_t S_{ij} * S_{ij} - C_{2\epsilon}\rho\frac{\epsilon^2}{k} \quad (12)$$

where k = turbulent kinetic energy, Nm

ϵ = dissipation rate μ_t = turbulent eddy viscosity, Ns/m^2

σ_k = Prandtl number for k σ_ϵ = Prandtl number for ϵ

$C_{1\varepsilon}$, $C_{2\varepsilon}$, and $C_{3\varepsilon}$ = model constants

The 5 terms in the equations above refer to changes in the k and epsilon terms. Eq. 11 in terms of words can be expressed by rate of change plus convection equals diffusion plus production minus destruction (Versteeg and Malalasekera, 2007).

The turbulent viscosity is modeled as

$$\mu_t = \rho C_\mu \frac{k^2}{\epsilon} \tag{13}$$

where C_μ is no longer constant as it is in the standard model and is computed by the following equations:

$$C_\mu = \frac{1}{A_0 + A_s \frac{kU^*}{\epsilon}} \tag{14}$$

$$U^* = \sqrt{S_{ij} S_{ij} + \Omega_{ij} \Omega_{ij}} \tag{15}$$

$$\Omega_{ij} = \Omega_{ij} - 2\epsilon_{ijk} \omega_k \tag{16}$$

$$\Omega_{ij} = \Omega_{ij} - \epsilon_{ijk} \omega_k \tag{17}$$

where Ω_{ij} is the mean rate of rotation tensor with an angular velocity of ω_k.

$$A_s = \sqrt{6} cos\emptyset \tag{18}$$

$$\emptyset = \frac{1}{3} cos^{-1}\left(\sqrt{6W}\right) \tag{19}$$

$$W = \frac{S_{ij} S_{jk} S_{ki}}{\hat{S}} \tag{20}$$

$$S = \sqrt{2 S_{ij} S_{ij}} \tag{21}$$

$$S_{ij} = \frac{1}{2}\left(\frac{\partial u_j}{\partial x_i} + \frac{\partial u_i}{\partial x_j}\right) \tag{22}$$

The model constants used are:

$$A_0 = 4.04 \quad C_{1\varepsilon}=1.44, \quad C_{2\varepsilon} = 1.9, \quad \sigma_\epsilon = 1.3 \quad \sigma_k = 1.0$$

The k-□ turbulence model was only used for flows with Re > 2,000, because the previous equations do not apply to non-fully turbulent pipe flows. For flows with a Re < 2,000 laminar flow was selected for the turbulence model, because with low flows the amount of uncertainty in flow behavior is greatly reduced and the k-epsilon equations are no longer needed.

All of the previous equations presented were computed internally by the FLUENT© software, while the following equations were computed by the author to determine the discharge coefficient from the FLUENT© results. The following general equation was used to determine the mass flow rate through the differential pressure flow meters (Miller, 1996).

$$q = N * \left[\frac{Cd^2}{\sqrt{1-(d/D)^4}} \right] * [Yf(\rho)] * \sqrt{h_w} \qquad (23)$$

The variables in Equation 23 can be separated into four different terms:

1) the dimensional constant N that relates the variable units (density d, density ρ, and differential head h_w) into the desired flow rate unit

2) Dimensional and viscosity dependent terms (Discharge Coefficient C, and Pipe Diameter D)

3) The Yf(ρ) term is density related, where in the case of gases, Y is the gas expansion factor and f(ρ) is the function of density

4) The measured differential head across the flow meter h_w

The Reynolds number equation below was used extensively and is a ratio of inertial forces to the viscous forces.

$$Re = \frac{V*D}{\upsilon} \tag{24}$$

where V = Average velocity through the pipe, m/s

D = diameter of pipe, m

υ = kinematic viscosity, m^2/s

The average velocity of a fluid through a closed conduit can be found using eq. 25.

$$V = \frac{Q}{A} \tag{25}$$

where Q = volumetric flow rate of fluid, L^3/t

A = cross sectional pipe area

Eq. 26 is the general discharge coefficient for a 90 degree wedge flow meter if the pipe diameter is greater than 3.81 cm, but is only accurate for Re's greater than 1000 (Miller, 1996). Fig. 3 demonstrates the general configuration of the wedge flow meter, as the segmental wedge is attached at the center of the meter with the pressure taps 1 and 2, each one pipe diameter away from the top edge of the wedge.

$$C = 0.5433 + 0.2453 * (1 - \beta_{wedge}^2) \tag{26}$$

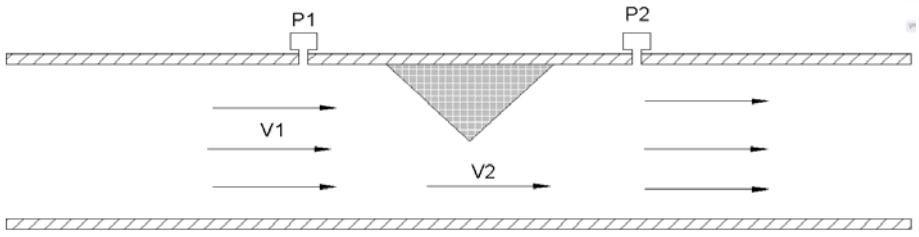

Fig. 3. Wedge flow meter.

The equivalent beta ratio of the wedge segment height H to diameter D is given below in Eq. 28 (Primary Flow Signal Inc., 2001).

$$\beta_{wedge} = \left(\frac{1}{\pi}\left\{arccos\left(1-\frac{2H}{D}\right) - 2 * \left(1-\frac{2H}{D}\right)\left[\frac{H}{D} - \left(\frac{H}{D}\right)^2\right]^{\frac{1}{2}}\right\}\right)^{\frac{1}{2}} \quad (27)$$

While the effective diameter, d for the wedge flow meter is

$$d_{wedge} = \beta * D \quad (28)$$

The wedge flow meter has a few primary advantages over other differential pressure flow meters including: there are no obstructions on the bottom of the pipe allowing for effective slurry and viscous fluid passage, pressure drops are small, and the ability to measure low flows at Re > 500 with a constant discharge coefficient (Banchhor et al., 2002).

Eq. 29 is used to determine the beta value for the standard orifice plate flow meter. Fig. 4 shows the general depiction of an orifice plate and how the streamlines contract/expand when flowing through the meter. The pressure taps for this study were placed 2.54 centimeters upstream and 2.54 centimeters downstream of the orifice plate for a flange tap differential pressure readings.

$$\beta_{orifice} = \frac{D_0}{D_1} \quad (29)$$

where D_o = the orifice plate diameter

D_1 = pipe diameter

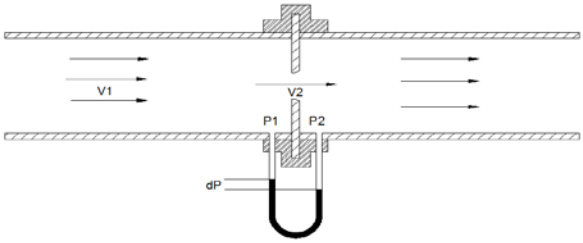

Fig. 4. Orifice flow meter.

Eq. 31 demonstrates how to calculate the beta value for a V-cone flow meter (McCrometer, 2002). Fig. 5 illustrates the general layout of a V-cone flow meter. The upstream pressure was measured just upstream of the device, while the downstream pressure was measured in various locations since there are multiple pressure inlets on the downstream face of the V-cone.

$$\beta_{v-cone} = \frac{\sqrt{D^2 - d_{cone}^2}}{D} \tag{30}$$

Eq. 31 shows the beta equation for a Venturi flow meter. Fig. 6 illustrates how the flow is gradually contracted into the throat section, and then gradually expands back to the pipe size to minimize head losses. A major benefit of this meter over many others is the relatively low head loss compared to other differential producers.

$$\beta_{venturi} = \frac{D_T}{D_I} \tag{31}$$

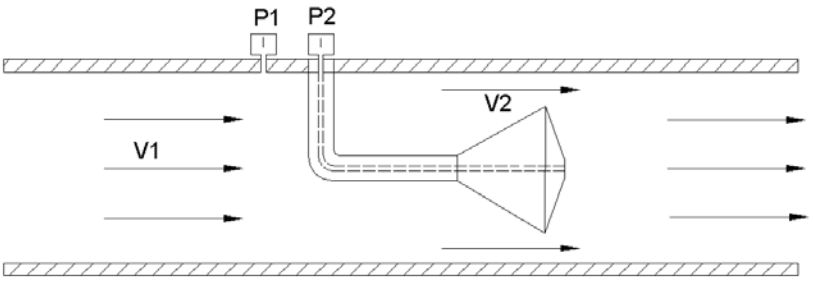

Fig. 5. V-cone flow meter.

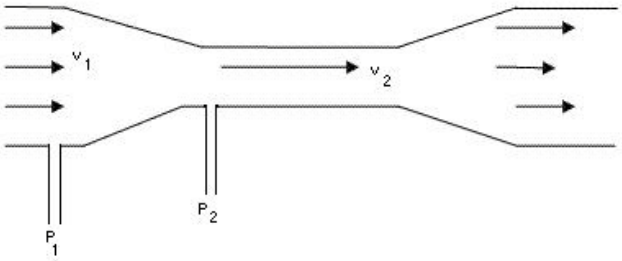

Fig. 6. Venturi flow meter.

Experimental procedure

Numerical model development and laboratory testing were performed at the Utah Water Research Laboratory. The primary computer used was a Dell Precision T3500 which had the following specifications: 6 GB Random Access Memory (RAM), two dual processors, a 64-bit operating system, 2 terabyte hard drives, and a Windows 7 Professional system. The models were created and meshed in GAMBIT© 2.4.6, then exported to FLUENT© 6.3.26. Each of the 12 models created were constructed in GAMBIT© with a top-down implementation. The geometries of the laboratory-tested flow meters were constructed to replicate the specified drawings that had been given to the UWRL for previous lab calibrations. After multiple simulations utilizing a varying upstream pipe length, it was determined that 10 diameters of upstream pipe ensured that the correct velocity profile was developed at the inlet of the meter.

Once the geometry of each model was constructed, meshing was applied to determine the points within the model where numerical computations would occur. After the testing of multiple meshing schemes, it was decided that the best fit for the geometries were tet/hybrid – Tgrid cells as shown in Fig. 7, while the rest of the meshes are shown in Appendix A. The mesh spacing was completed by using the interval count

method scheme, where the initial input number varied based on the diameter and geometry of the flow meter being used. The goal of the meshing procedure used by the authors was to create the most accurate results by creating the finest possible mesh, while eliminating skewness greater than 0.97 in the resulting cells. Once the models had been meshed, there were up to 600,000 computational cells in a model.

Defining boundary conditions is one of the most important processes for each of the models created in GAMBIT©. The flow inlet on the 10-diameter upstream pipe was defined as the velocity inlet, while the exit of the flow meter was defined as a pressure outlet. All other faces in the geometry were identified as walls. The velocity inlet boundary condition was applied, so that the measured flow from the lab data could be used for comparison purposes. The pressure outlet condition was employed to ensure that with different fixed outlet pressures the differential pressure through the meter would be unaffected. Once the boundary conditions had been applied to all of the faces of a model it was then saved and exported as a mesh to be opened in FLUENT©.

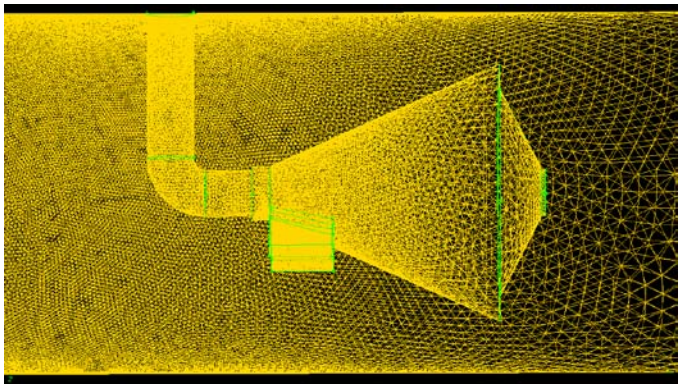

Fig. 7. Tgrid mesh of V-cone flow meter.

FLUENT© was then opened and the case file for the mesh was read. Since the models were three dimensional and double precision (3ddp) was to be used the 3ddp option was selected when opening FLUENT©. The tet/hybrid cells shown in Fig. 8 were converted to polyhedral cells to significantly reduce computation time normally associated with hybrid cells. Models were scaled from the default measurement of meters into inches for appropriate sizes to be used in association with the flow meters being replicated in the study. Performing a check on the mesh after the cell type conversion was important to help identify any problems with the mesh that could adversely affect the results. Through the completion of many test runs the authors determined that the best viscous turbulence model for this study was the realizable k-epsilon model with the standard wall function enabled. This particular model was used for any runs that had a Reynolds number greater than 2,000. The laminar viscosity model was used for any of the models that had a Re of 2,000 or less. All the constants associated with this version of FLUENT© were left at their default values unless otherwise specified.

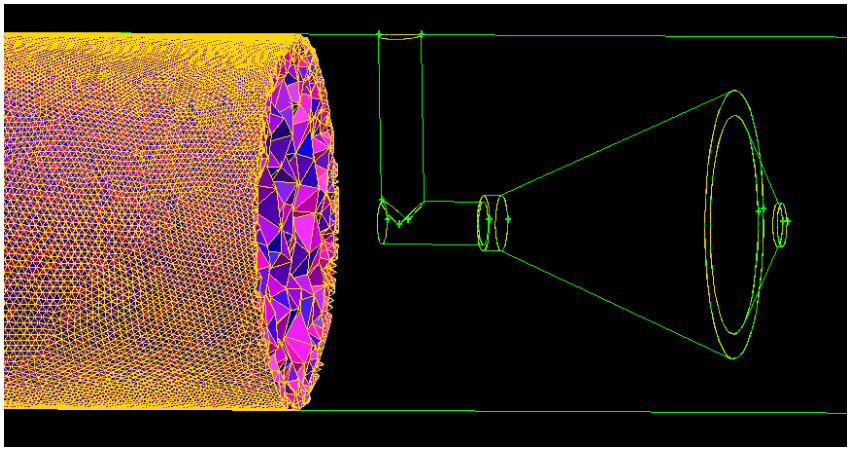

Fig. 8. 3D view of tet-hybrid cells approaching V-cone.

Operating conditions were taken into consideration to mimic lab data results. The operating atmospheric pressure was set to 88.9 kPa based on the relative UWRL elevation, while gravitational acceleration was also taken into consideration. Boundary condition specifications are one of the most significant aspects to be carefully determined when creating a model. The study included heavy oil and water as the two different types of fluids to be examined in order to obtain data for the entire range of Reynolds numbers. Water was used for the large Re so that numerical results could be directly compared to actual laboratory data; while oil was used for the small Re numbers being examined. The primary difference between the two fluids was that the viscosity of the oil was much greater than that of water to ensure larger pressure differences at small Re. The velocity inlet condition only required the calculated velocity based on predetermined Reynolds numbers. All of the input velocities for each of the runs are shown in Appendix B. The velocity specification method used in this study was the magnitude of the velocity normal to the boundary, while there was an absolute reference frame. The pressure outlet was usually set anywhere from 35-70 gauge kPa to replicate normal downstream pressures. The simulations performed the same whether 35 or 69,000 gauge kPa was used for the downstream pressure outlet. It is important to observe when studying the results that potential cavitation is not taken into account using FLUENT©, therefore high negative pressures are not a cause for concern.

The pressure velocity coupling used was the Simple Consistent algorithm with a skewness correction of 0. The Under-Relaxation Factors were set to 0.4 for all of the variables besides the pressure factor which was set to 0.9 (Spall, personal communication, 2010). Discretisation factors are vital when regarding the accuracy of

the numerical results. For this study standard pressure was used, while the Second-Order Upwind method was applied for momentum, kinetic energy, and the turbulent dissipation rate.

Residual monitors were used to determine when a solution had converged to a point where the results had very little difference between successive iterations. When the k-epsilon model was applied, there were six different residuals being monitored which included: continuity, x, y, and z velocities, k, and epsilon. The study aimed to ensure the utmost iterative accuracy by requiring all of the residuals to converge to 1e-06, before the model runs were complete. The pressure based algorithm shown in Fig. 9 demonstrates the process in which the computer found the correct fluid properties for each grid point.

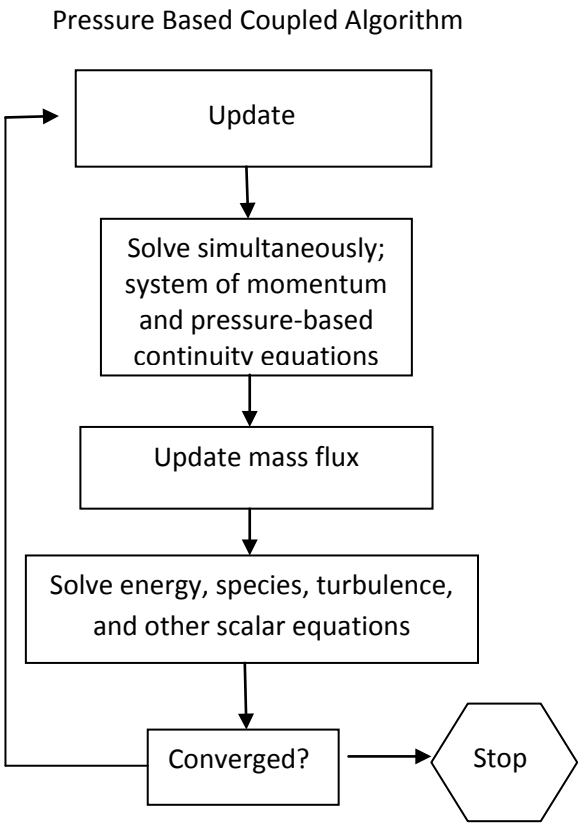

Fig. 9. Pressure coupled based algorithm.

Surface planes were created to determine resultant pressures at each of the flow meter's pressure tap locations. The planes were cross-sectional views located at both of the taps for each model except for the V-cone flow meter. The V-cone models were treated differently, because the downstream pressure was the average pressure on the backside of the cone as there were multiple pressure inlets. In each of the model cross-sections, average pressures were taken from the wall boundary computational points to determine the theoretical pressure at the taps. Fig. 10 shows the pressure results of a wedge flow meter simulation with the surface planes visible.

The models were initialized with the input velocity to ensure that the initial iterations gave plausible results. During the initialization, there were usually at least 10 iterations performed on the computer while the residuals were plotted and monitored for any unusual increases. Once the iterations were completed, the initial results were viewed to ensure all boundary conditions were performing properly and no other obvious errors were present.

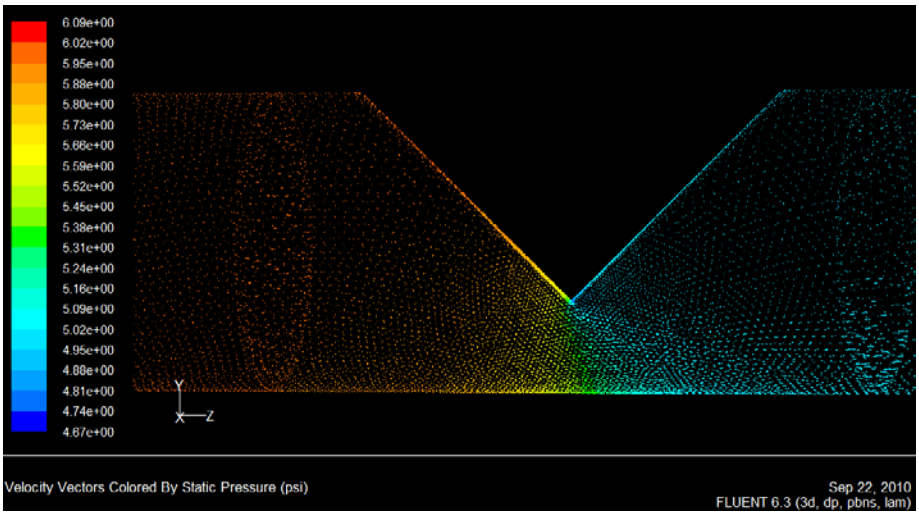

Fig. 10. Wedge flow meter with surface planes.

Since the CPU time required to solve the models was quite excessive, it was decided that the HPC Cluster at USU would be utilized to reduce computational time. After the initialization of the models, they were transported to the cluster using a WinSCP program. Once on a cluster directory, a job script was created for each run and then submitted to be computed on the cluster. Once the job had been completed, the data file was available to transport back to the Dell computer being used. With the case and data files complete for a model run, the results could then be analyzed using FLUENT©. All processes on the cluster were run on 16 processors to dramatically reduce local computational time that would have otherwise been required.

Experimental results

It was determined that the best way to present the data for it to be easily interpreted for the meters investigated was to provide the discharge coefficient vs. Reynolds number plots on semi-log graphs. Each of the data points on the graphs was computed separately based on the performance from a pre-determined Reynolds number. The data was separated into four different graphs with respect to the flow meter being represented. Lab data was also provided for the models on the same graphs. The velocities that were needed to obtain different Re values were the primary variable put into the numerical model when computing each meters discharge coefficients. Heavy Oil was used for flows where Re < 20,000 while water was used for higher turbulent flow test runs. To be sure the procedure used was accurate, both water and heavy oil were run at a Re of 20,000, and resulting C's for each fluid were within 0.2% from one another and within 3% of the lab data.

Two different Venturi models were used to acquire discharge coefficient data as shown in Fig. 11. Both of the Venturis had an inside diameter of 15.405 centimeters, and a beta value of 0.661. The primary difference between the two modeled Venturis was their respective inlet geometries. In one case the inlet smoothly transitioned to the throat using a parabolic cone and the other had what might be described as a segmented cone having two break points as it reduced from the inlet to the throat.

Four standard orifice plate models with different beta values were modeled to better understand the beta vs. discharge coefficient relationship as revealed in Fig. 12. The following common beta values were used to model orifice plates: 0.50, 0.60, 0.65, and 0.70. Flow meter sizes ranged from 15.41 to 20.27 centimeters, to determine if there were any resulting differences depending on the meter's inlet diameter.

Three V-cone models were developed to demonstrate discharge coefficient data. The different beta values used for the models were 0.6611, 0.6995, and 0.8203 while their respective flange diameters were 30.67, 25.75, and 30.69 centimeters as shown in Fig. 13.

Three wedge flow meter models were created to determine their discharge coefficient data for a wide array of Reynolds numbers. Two of the three models had the same beta value of 0.5023 (H/D = 0.3) and different diameters to observe if there was any significant difference in results based on pipe diameter. The other beta value tested was 0.611(H/D = 0.4) for a wedge flow meter with a 20.27-centimeter inner diameter as shown in Fig. 14. All of the models that were tested can be seen in the summary Table 1.

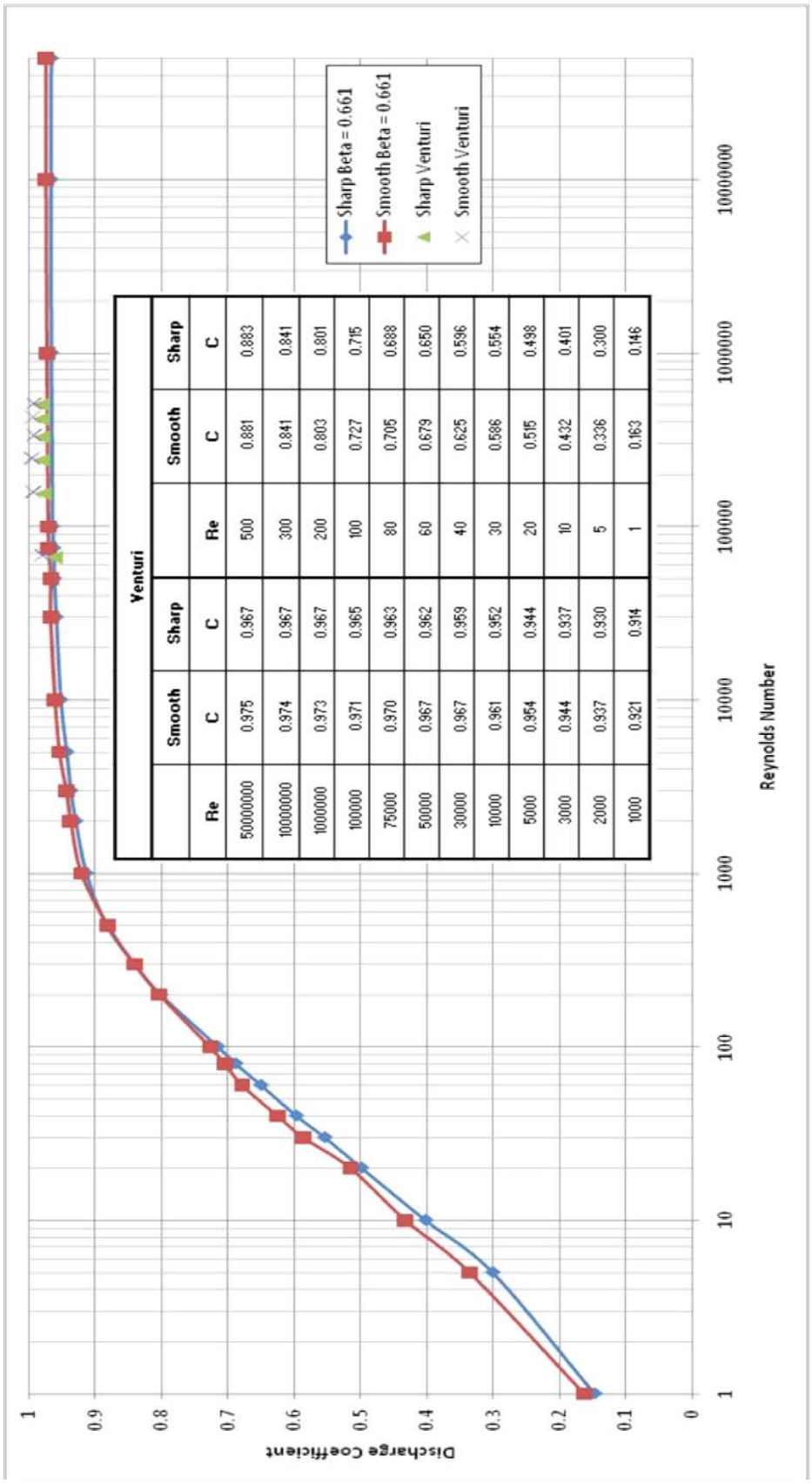

Venturi						
	Smooth	Sharp		Smooth	Sharp
Re	C	C	Re	C	C
50000000	0.975	0.967	500	0.881	0.883
10000000	0.974	0.967	300	0.841	0.841
1000000	0.973	0.967	200	0.803	0.801
100000	0.971	0.965	100	0.727	0.715
75000	0.970	0.963	80	0.705	0.688
50000	0.967	0.962	60	0.679	0.650
30000	0.967	0.959	40	0.625	0.596
10000	0.961	0.952	30	0.586	0.554
5000	0.954	0.944	20	0.515	0.498
3000	0.944	0.937	10	0.432	0.401
2000	0.937	0.930	5	0.336	0.300
1000	0.921	0.914	1	0.163	0.146

Fig. 11. Venturi discharge coefficients.

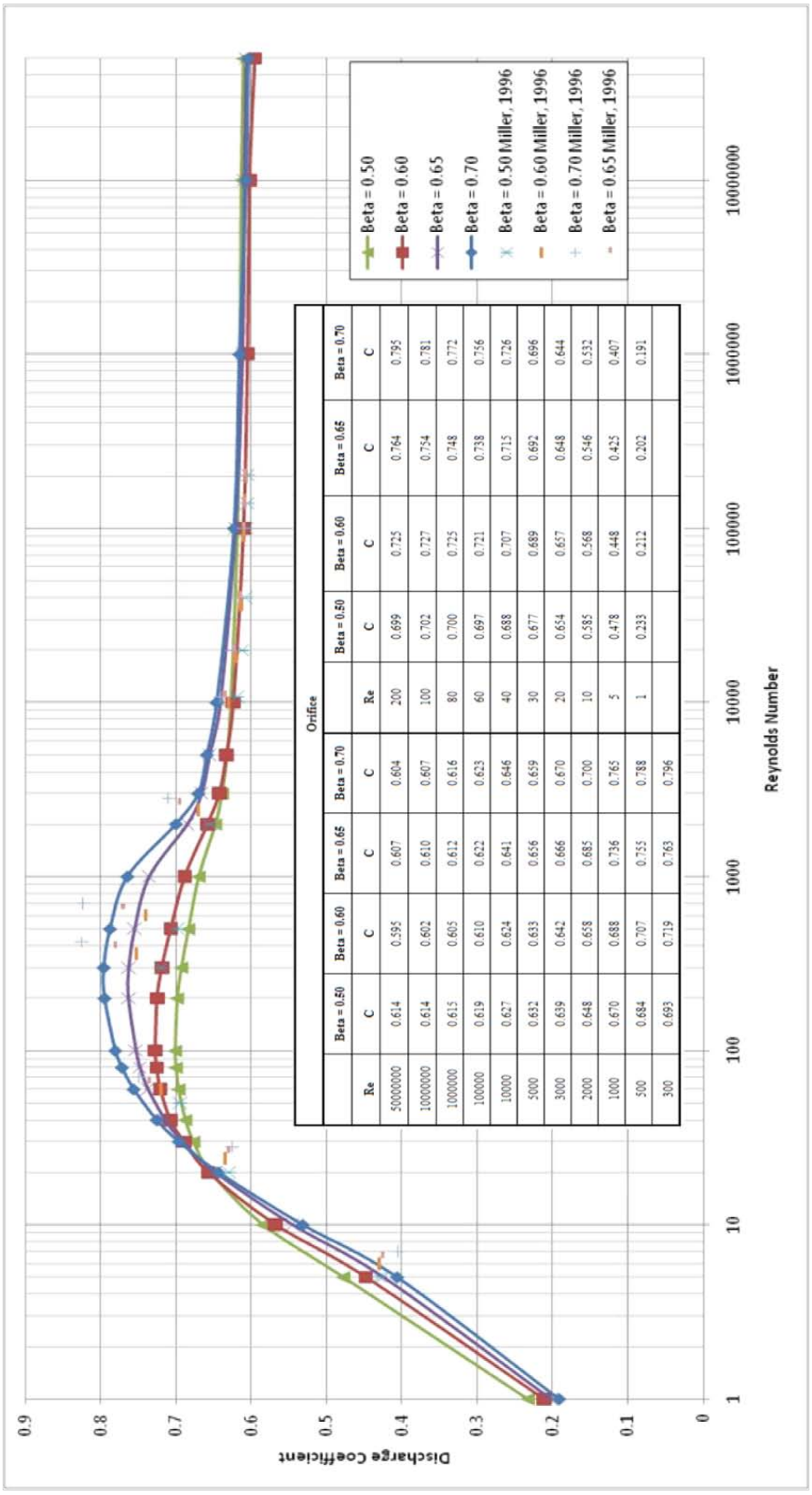

Orifice

Re	Beta = 0.50 C	Beta = 0.60 C	Beta = 0.65 C	Beta = 0.70 C
50000000	0.614	0.595	0.607	0.604
10000000	0.614	0.602	0.610	0.607
1000000	0.615	0.605	0.612	0.616
100000	0.619	0.610	0.622	0.623
10000	0.627	0.624	0.641	0.646
5000	0.632	0.633	0.656	0.659
3000	0.639	0.642	0.666	0.670
2000	0.648	0.658	0.685	0.700
1000	0.670	0.688	0.736	0.765
500	0.684	0.707	0.755	0.788
300	0.693	0.719	0.763	0.796

Re	Beta = 0.50 C	Beta = 0.60 C	Beta = 0.65 C	Beta = 0.70 C
200	0.699	0.725	0.764	0.795
100	0.702	0.727	0.754	0.781
80	0.700	0.725	0.748	0.772
60	0.697	0.721	0.738	0.756
40	0.688	0.707	0.715	0.726
30	0.677	0.689	0.692	0.696
20	0.654	0.657	0.648	0.644
10	0.585	0.568	0.546	0.532
5	0.478	0.448	0.425	0.407
1	0.233	0.212	0.202	0.191

Fig. 12. Standard orifice plate discharge coefficients.

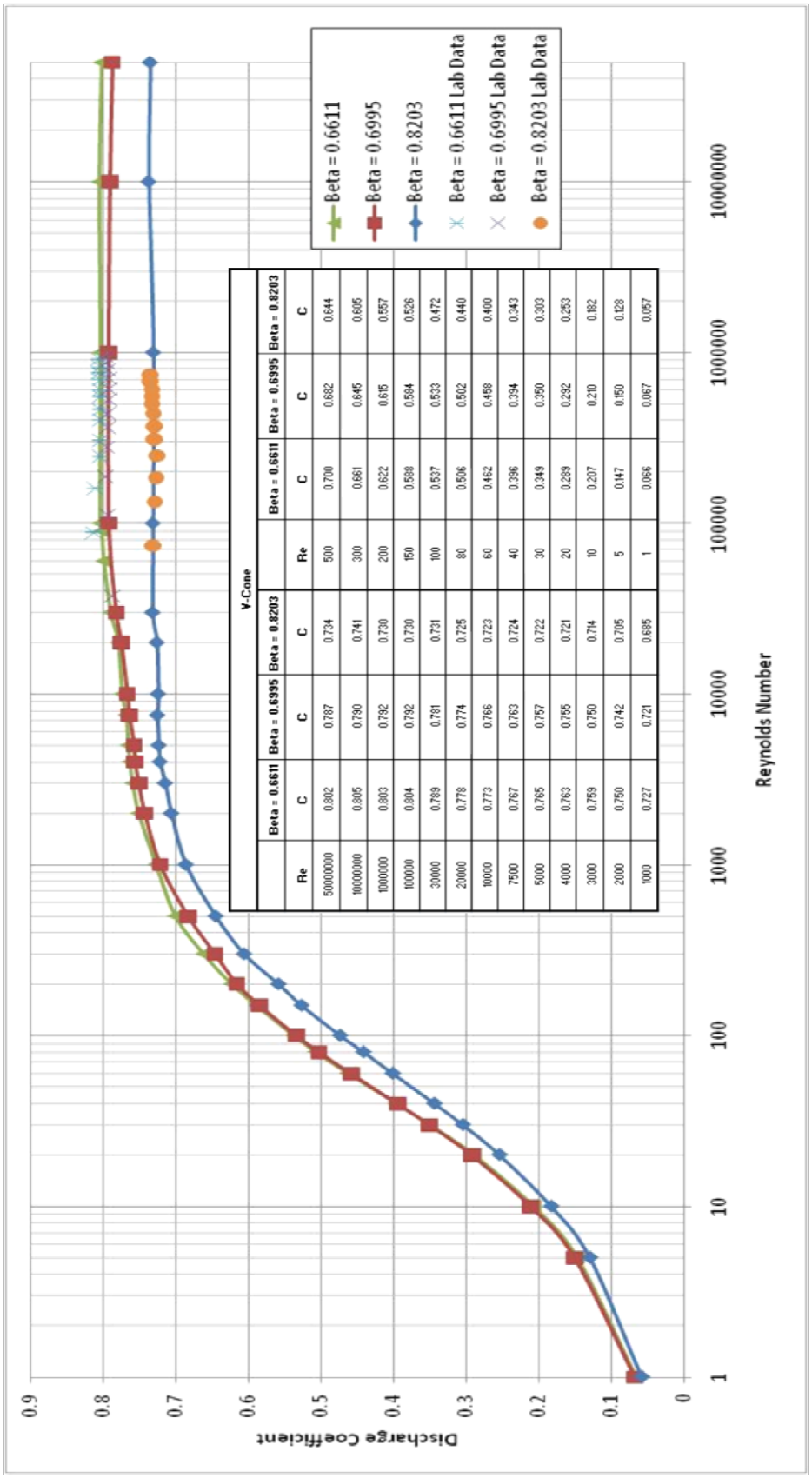

V-Cone

	Beta = 0.6611	Beta = 0.6995	Beta = 0.8203		Beta = 0.6611	Beta = 0.6995	Beta = 0.8203
Re	C	C	C	Re	C	C	C
50000000	0.802	0.787	0.734	500	0.700	0.682	0.644
10000000	0.805	0.790	0.741	300	0.661	0.645	0.605
1000000	0.803	0.792	0.730	200	0.622	0.615	0.557
100000	0.804	0.792	0.730	150	0.588	0.584	0.526
30000	0.789	0.781	0.731	100	0.537	0.533	0.472
20000	0.778	0.774	0.725	80	0.506	0.502	0.440
10000	0.773	0.766	0.723	60	0.462	0.458	0.400
7500	0.767	0.763	0.724	40	0.396	0.394	0.343
5000	0.765	0.757	0.722	30	0.349	0.350	0.303
4000	0.763	0.755	0.721	20	0.289	0.292	0.253
3000	0.759	0.750	0.714	10	0.207	0.210	0.182
2000	0.750	0.742	0.705	5	0.147	0.150	0.128
1000	0.727	0.721	0.695	1	0.066	0.067	0.057

Fig. 13. V-cone flow meter discharge coefficients.

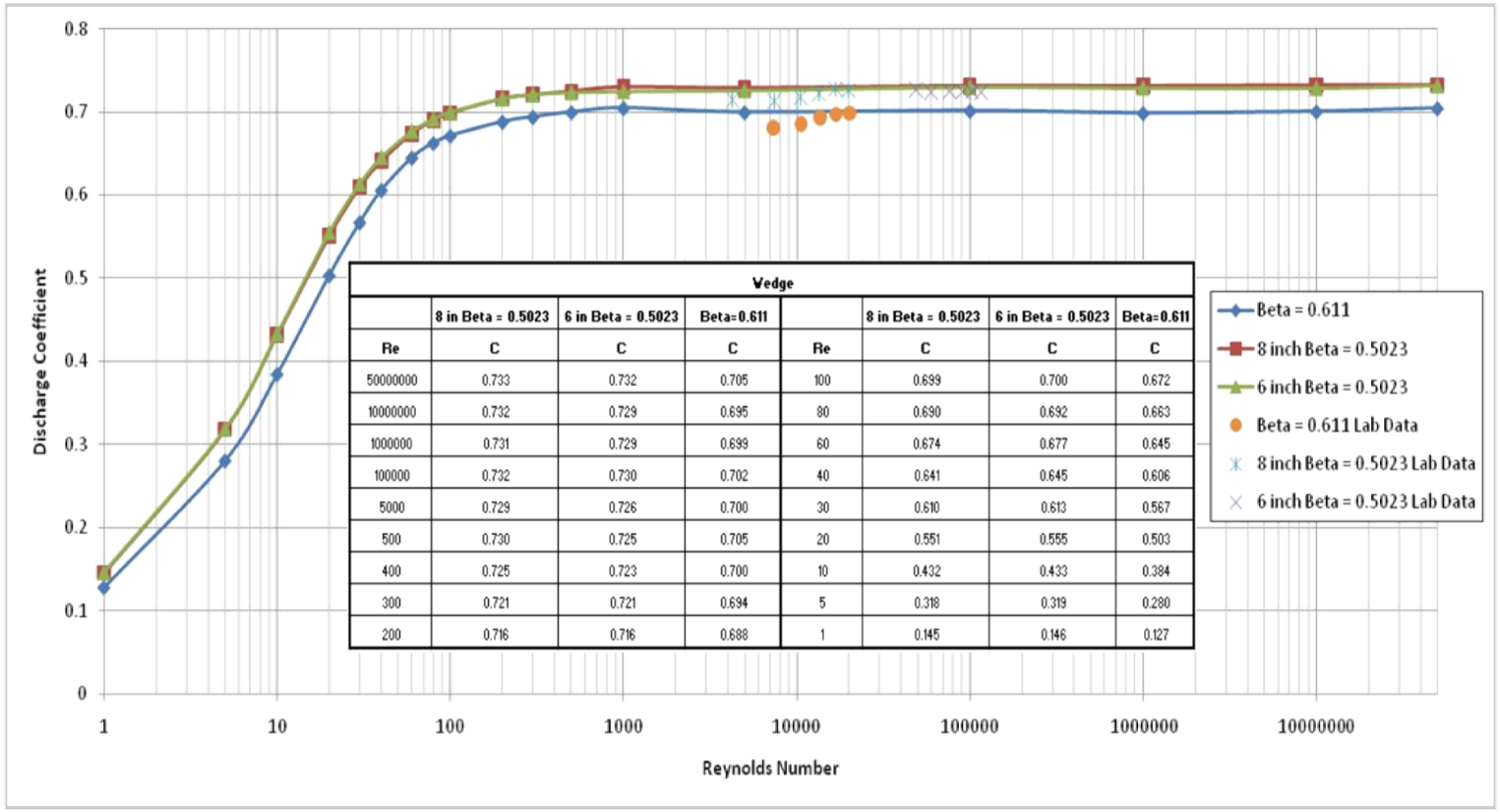

Wedge							
	8 in Beta = 0.5023	6 in Beta = 0.5023	Beta=0.611		8 in Beta = 0.5023	6 in Beta = 0.5023	Beta=0.611
Re	C	C	C	Re	C	C	C
50000000	0.733	0.732	0.705	100	0.699	0.700	0.672
10000000	0.732	0.729	0.695	80	0.690	0.692	0.663
1000000	0.731	0.729	0.699	60	0.674	0.677	0.645
100000	0.732	0.730	0.702	40	0.641	0.645	0.606
5000	0.729	0.726	0.700	30	0.610	0.613	0.567
500	0.730	0.725	0.705	20	0.551	0.555	0.503
400	0.725	0.723	0.700	10	0.432	0.433	0.384
300	0.721	0.721	0.694	5	0.318	0.319	0.280
200	0.716	0.716	0.688	1	0.145	0.146	0.127

Fig. 14 . Wedge flow meter discharge coefficients.

Table 1
Summary of flow meter geometries tested.

Summary Table of Meters Tested					
Type	**Diameter (cm)**	**Beta Value**	**Type**	**Diameter (cm)**	**Beta Value**
Venturi	15.41	0.6610	**V-Cone**	30.67	0.6611
"	15.41	0.6610	"	25.75	0.6995
Orifice	15.41	0.5000	"	30.69	0.8203
"	20.27	0.6000	**Wedge**	15.41	0.5023
"	15.41	0.6500	"	20.27	0.5023
"	15.41	0.7000	"	20.27	0.6110

The Reynolds numbers for the previous figures are presented on the x axis in a logarithmic approach since there is such a wide array of numbers being presented. The discharge coefficients are on the normally plotted y axis where the values range from 0-1.

Using the results

Figs. 11 through 14 demonstrate that the characteristics of the flowing fluid must be known before calculations can be completed such as, meter geometry, viscosity, and measured differential head. The viscosity can be found in published tables or by using either a viscometer or a rheometer depending on the fluid being measured (Bandyopadhyay and Das, 2007). This information is needed to obtain an estimation of the average Reynolds number flowing through the flow meter pipeline in question using Eq. 25.

The following example problem shows how the previous figures can be used to obtain a correct flow. For this particular example a wedge flow meter will be used, but the same process can be used for any of the flow meters in the study, with only the beta equation being the primary variation.

$$q = N * \left[\frac{C*d^2}{\sqrt{1-(d/D)^4}}\right] * [Yf(\rho] * \sqrt{h_w} \quad (32)$$

$$N_{lps} = \frac{\pi}{4} * \sqrt{2 * 9.81} * \frac{1000}{10{,}000*\sqrt{100}} = 0.03479 \quad (33)$$

$$\beta_{wedge} = \left(\frac{1}{\pi}\left\{arccos\left(1-\frac{2H}{D}\right) - 2 * \left(1-\frac{2H}{D}\right)\left[\frac{H}{D} - \left(\frac{H}{D}\right)^2\right]^{\frac{1}{2}}\right\}\right)^{\frac{1}{2}} \quad (34)$$

To show how one could use the data, assume a pipeline with a diameter (D) of 15.41 centimeters, which transports heavy oil with a viscosity of $2.64*10^{-4}\ \frac{m^2}{sec}$ (υ). The differential pressure flow meter being used is a wedge flow meter with an H/D ratio of 0.4. It is observed that the differential head being produced by the flow meter is 1.27 centimeters. The process to obtain the flow rate through the flow meter is as follows:

1: Determine the β value, N constant, and d for the particular flow meter and units in question:

$\beta_{wedge} = \left(\frac{1}{\pi}\left\{arccos(1-2*0.4) - 2*(1-2*0.4)[0.4-(0.4)^2]^{\frac{1}{2}}\right\}\right)^{\frac{1}{2}} = 0.6111$

d = 15.41*0.6111 = 9.42

2: Guess Re (can get reasonably close by noticing pressure differential):

Re = 1,000

3: From relevant figure, for this case Fig. 13, obtain a C from the discharge coefficient curve for similar beta values: Re = 1000, C = 0.70.

4: Calculate Q in liters per second using equation 32:

$Q_{lps} = 0.034788 * \left(\frac{0.70*(9.42)^2}{\sqrt{1-0.6111^4}}\right) * \sqrt{1} * \sqrt{1.27} = 2.625\ lps$

5: Calculate the average pipe velocity by dividing the flow in cms by the pipe area:

$$V = \frac{\frac{2.625}{1000}}{0.01865} = 0.141\ m/s$$

6: Compute the new Reynolds number with Eq. 25:

$$Re = \frac{0.141 * 0.1541}{2.636 * 10^{-4}} = 82.4$$

7: Use the computed value from step 6 and repeat the iterative process steps 3 through 6 until the estimated flow no longer fluctuates significantly. For this example, 4 iterations resulted in a flow of 2.513 lps. The solution of Eq. 32 and curve from Fig. 13 converged to a flow of 2.475 lps.

It is significant to observe that using the correct discharge coefficient is vital, as for this example if the normal C = 0.70 is used rather than the calculated C = 0.66 it would have resulted in a theoretical Q of 6.1% more flow than the true iterative value. The varying discharge coefficient is obviously an essential parameter for accurate measurement of small Re flows.

The aforementioned process is similar for the other three differential pressure flow meters in the study, except the beta equation for each meter is different as demonstrated in Eqs. 28-31.

Uncertainty of results

Uncertainty in numerical results cannot be overlooked when using computational fluid dynamics as a problem solver. Discretisation errors are one of the primary errors to consider when analyzing CFD results including both spatial and temporal (Celik et al., 2008).

The discretisation errors for each of the models were found using a common procedure for estimation and reporting uncertainty using CFD (Celik et al., 2008). To

implement this procedure three vastly different grid generations were created for each of the models to verify grid convergence results. Once the different grids had been created for each model, they were run with the same boundary conditions to determine differences in the resultant discharge coefficient. When the three different coefficients were determined for a model the rest of the equations in the procedure could be calculated to determine the approximate error, extrapolated error, and grid convergence index error. The largest of the calculated errors was the suggested numerical error for the model. The study determined that throughout 12 experiments that 42% of the results were within 1%, 83% within 2%, and 95% within 2.5%. Table 2 shows the summarized errors. The procedural results for each of the models can be found in Appendix C.

The lab data that was used for numerical comparison in the study had a numerical uncertainty of 0.5%.

Table 2
Summary of model discretisation uncertainty.

Discretisation Numerical Uncertainty				
	Venturi	**Orifice**	**V-Cone**	**Wedge**
Maximum Errors:				
Approximate	0.65%	1.34%	0.83%	1.13%
Extrapolated	0.71%	0.29%	2.33%	2.17%
GCI	1.10%	0.08%	2.15%	0.64%

Recommendations/further research

The results from this study could be expanded with future research of discharge coefficients of differential pressure flow meters. An area of possible interest is to use boundary layers on the model walls when generating the model mesh in GAMBIT©. This will help to ensure the accuracy of using the enhanced near wall treatment option for the k-epsilon model rather than the standard wall treatment as was used in this study.

An additional area of potential interest is performing tests over a wide range of beta values to obtain a more complete understanding of discharge coefficient relationships. This study only focused on a few of the most common beta values that are used in industries today, but the knowledge from this study could be expanded to determine more complete relationships for beta values and C's. Additional types of differential pressure flow meters could also be modeled in the same fashion as the ones in this study to determine how they perform at small Reynolds numbers.

CHAPTER IV

DISCUSSION

There are many pipelines where flows need to be accurately measured. Meters having a high level of accuracy and relatively low cost are a couple of the most important parameters when deciding on the purchase of a flow meter. Most differential pressure flow meters meet both of these requirements. Many of the most common flow meters have a specified range where the discharge coefficient may be considered constant and where the lower end is usually the minimum recommended Re number that should be used with the specified meter. With the additional knowledge of this study it will enable the user to better estimate the flow through a pipeline over a wider range of Reynolds numbers.

The research completed in this study on discharge coefficients focused on four different types of flow meters with varying beta ratios. The resultant discharge coefficients should only be used for similar geometries to those used in the study and not for those which vary greatly, but the results should follow a similar trend. A complete analysis on the effect of varying beta ratios was not completed, so the results of this study should only be applied as possible trends to differing beta values.

The Venturi meter was modeled using two slightly different geometries to determine if there was significant effect on the resultant C's over the Re range. It was found that both of the data sets followed very similar trends despite having different geometries. The flow meter that had the parabolic converging cone, which creates less turbulent losses than the segmented converging, had a slightly larger C throughout the Re

range simulated. The beta value tested for both meters was 0.661 for a 6.065-inch pipeline. In the study it was found that the discharge coefficient C remained fairly constant varying less than 1 % for Reynolds numbers between 75,000 and 50,000,000. As the Re numbers went from 30,000 to 1, the values dropped from 0.96 to 0.15 on the semi-log plot shown in Fig. 10.

The standard concentric orifice plate was modeled using four different beta ratios and compared to Miller's data (Miller, 1996). The study concluded that the C vs. Re for this flow meter responded unlike the other three flow meters, because the discharge coefficient is not constant and varies with the Re unlike the other flow meters investigated. Though there is no constant C, there has been a significant amount of research on orifice plates conducted to determine the discharge coefficient characteristics for Re greater than 10,000. In the study for Reynolds numbers less than 10,000 the discharge coefficients increase to a Re of approximately 300 and then reduce, which is attributed to an orifice plate's effect on the velocity profile (Britton and Stark, 1986). Since the highest velocities in a smooth pipe are located in the center, the small Re numbers have a larger C because most of the velocity associated with the flow passes through the flow meter without being as affected by the orifice plate at larger Re (Britton and Stark, 1986). For Re numbers trending from 100-1, the resultant C reduces from 0.7-0.8 to 0.2-0.25 depending on the beta ratio of the meter.

The V-cone flow meter was modeled using three different beta values. It was determined that as the beta values increased from 0.66 to 0.82 that the corresponding C values dropped from 0.803 to 0.731. For the constant discharge coefficient the V-cone

meter derivations appeared to be similar to that of the Venturi meter with a variance of less than 1% for the Re range of 30,000 to 50,000,000.

The wedge flow meter was modeled using two different beta values. Two different pipe sizes were used with the same beta to determine if there was any significant relationship between discharge coefficients and flow meter size. The results showed there to be relatively no difference between the two models that had similar beta values and different inlet diameters. The wedge flow meter's constant discharge coefficient had a variance within 1% ranged from $500 < Re < 50{,}000{,}000$. Reynolds numbers from 500 to 1 had a C values ranging from 0.725-0.70 to 0.146-0.127 respectively depending on the beta value used. The larger beta values resulted in a decrease in the constant discharge coefficient because as beta increases so too does H/D. As the segmental wedge becomes larger relative to the pipe diameter, it creates a larger pressure differential for similar flows and more energy is lost due to turbulence on the backside of the wedge, therefore decreasing the constant C.

Table 3 compares the calculated flow rates with and without differing discharge coefficients for the flow meters that are often assumed to have constant discharge coefficients. Table 3 shows the rapid increase in percent difference between the two calculated flow rates as the Reynolds number decreases due to the decreasing discharge coefficient.

Table 3
Comparison of flow rates with and without varying discharge coefficients.

Reynolds Number	Flow Rate Venturi w/ constant C (gpm)	Flow Rate Venturi w/ varying C (gpm)	% difference constant C to varying C	Flow Rate V-Cone w/ constant C (gpm)	Flow Rate V-Cone w/ varying C (gpm)	% difference constant C to varying C	Flow Rate Wedge w/ constant C (gpm)	Flow Rate Wedge w/ varying C (gpm)	% difference constant C to varying C
100000	298.65	297.66	0.33%	500.88	499.91	0.19%	328.72	330.42	-0.51%
10000	5218.58	5156.89	1.20%	10487.22	10066.79	4.18%	3342.19	3326.84	0.46%
5000	2638.95	2578.44	2.35%	5301.67	5033.4	5.33%	658.69	665.37	-1.00%
500	336.39	257.84	30.46%	579.15	503.34	15.06%	331.78	332.68	-0.27%
100	69.51	51.57	34.79%	151.05	100.67	50.04%	69.1605	66.54	3.94%
10	12.38	5.15688	140.07%	39.21	10.0667	289.50%	12.09	6.65	81.80%
1	3.3881	0.515688	557.01%	12.33	1.0066	1124.92%	3.6475	0.6653	448.25%

The general trends of the discharge coeffiecients can be observed in Fig. 15 over a large range of Reynolds numbers. The figure shows the percentage of flow reduction if a constant C were assumed for each of the flow meters in the study. For example if V-Cone flow meter had a Re of 10 passing through it, the percent differnce between the flow using a constant C of 0.73 and the numerical C of 0.18 would result in 78% less flow through the meter. Positive y axis values indicate flow reduction, while negative values represent additional flow.

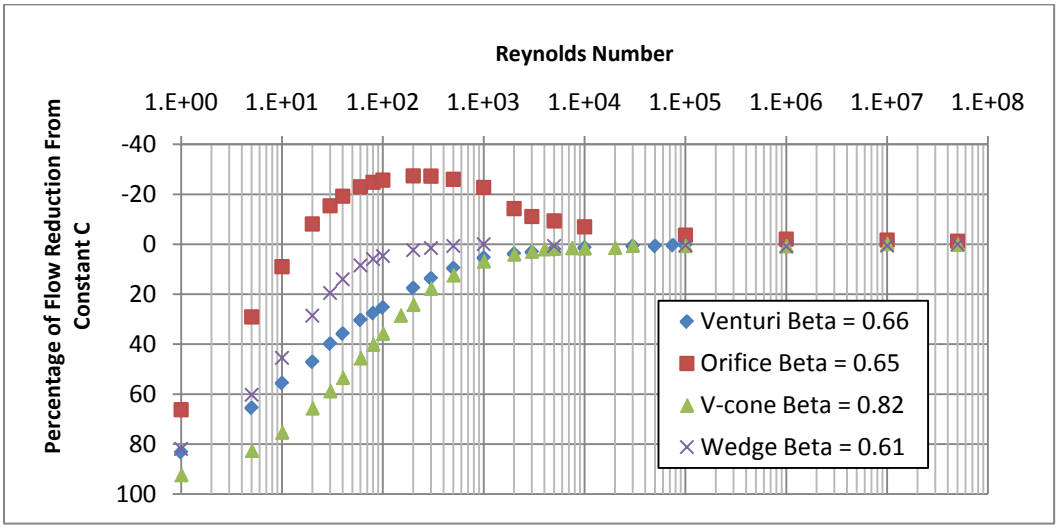

Fig. 15. General trend of discharge coefficients.

As shown in Fig. 15 all of the meters have a flow reduction as the Reynolds number decreases, besides the orifice plate where the actual flow increases down to a Reynolds number of 200. Table 3 shows that each of the three flow meters above have different lower limits to where a constant C is safe to assume. The wedge flow meter remained the most constant only varying within 1% for flows above Re of 500. For the other extreme it is shown that the V-cone flow meter has over an error of over 1120% at the lowest end if a constant C were assumed to be true at an Re = 1.

The data presented by Miller's 2008 physical study for Venturi flow meters were compared to the results of this study of which both were comparable (Miller et al., 2009). Since the exact geometry of Venturi used in Miller's experiment was not known the results shown in Fig. 16 vary.

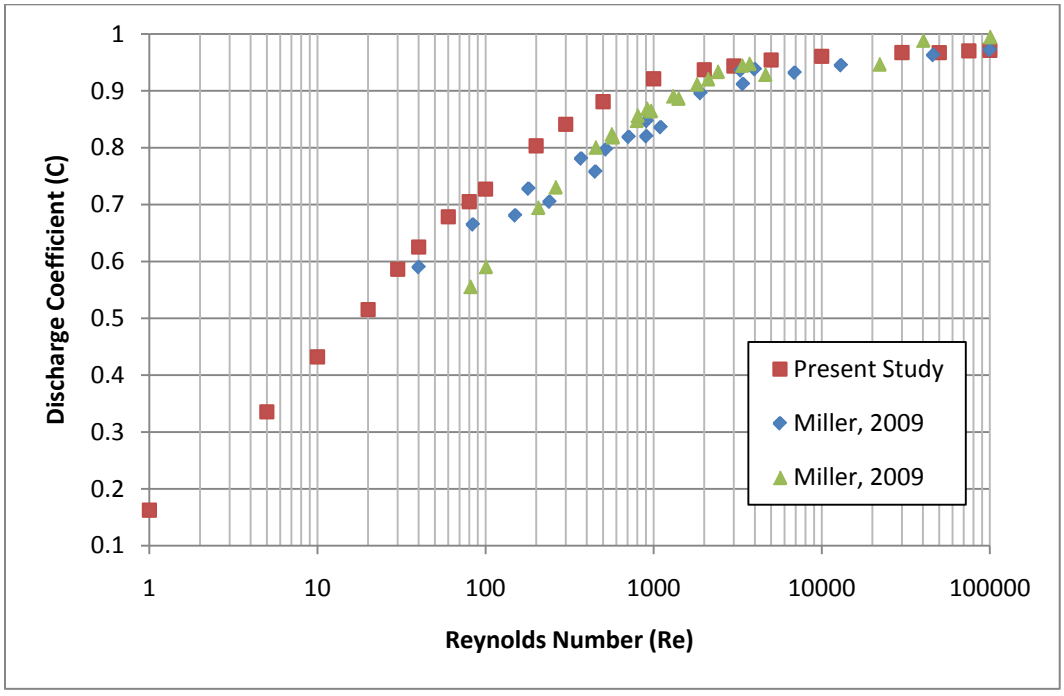

Fig. 16. Venturi flow meter data.

Miller et al. (2009) used a multiphase flow of heavy oil and water through the Venturi meters tested, which may be the reason that the C values decrease more rapidly than the present study data suggests. If the multiphase flow was not completely mixed, some of the oil may settle at the entrance of the ventrui meter, and result varying C's. With a maximum C variance of 21% between Millers heavy oil study and the present study at a Re of 80, shows there to be increasing uncertainty in the lab data. Since multiphase flows do not usually perform as a single phase fluid through pipelines as in the authors study it is likely to be the primary reason for the difference.

Singh's study presented data for V-cone flow meters and their average C over a range of Re numbers from 2,000 to 100,000 (Singh et al., 2006). Singh performed a series of physical tests and found there to be a near constant discharge coefficient. Fig. 17 shows the Singh V-cone study averages for two different beta values and the present study data for three different beta values.

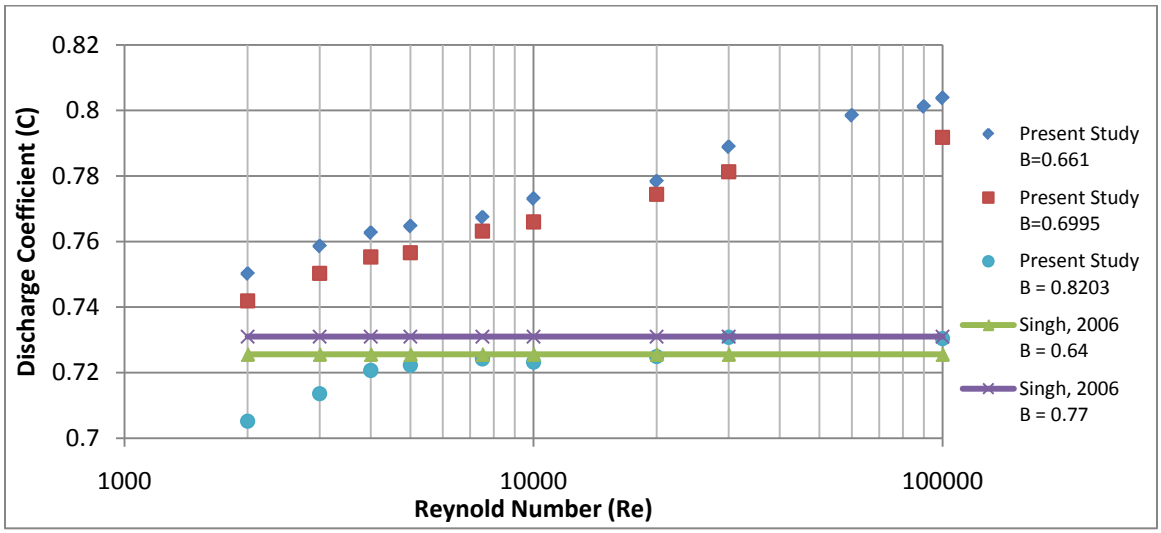

Fig. 17. V-cone flow meter data.

As demonstrated in Fig. 17, actual data points for the present study are shown while only averages from Singh study were available. Singh's averages show there to be little difference in resulting C value for beta values of 0.64 and 0.77, while the present study suggests there to be a larger difference. This could be a result of differing V-cone geometries as there are many different types of V-cone meters in the industry. Not all V-cone flow meters measure pressure differences in the same way on the downstream face as there is no designated pressure tap location. For the present study averages were taken on the D.S. face of the V-cone as there were multiple pressure inlets on the face. Singh's data suggests that as the beta value increases so too does the discharge coefficient, while the present study suggests the opposite.

Banchhor (Banchhor et al., 2002) and Yoon (Yoon et al., 2007) studied the characteristics of wedge flow meters under varying conditions. Banchhor used FLUENT© to collect numerical data, while Yoon used physical data. Table 4 shows the average discharge coefficients for the two H/D values and their differences presented in the literature and the present study.

Table 4
Wedge coefficient differences between literature and the present study.

		Present	Yoon	
Re Range	H/D	Study C	Study C	% difference
500-100000	0.3	0.731	0.813	11.22%
500-100000	0.4	0.699	0.797	14.02%
		Present	Banchhor	
Re Range	H/D	Study C	Study C	% difference
500-100000	0.4	0.699	0.681	2.58%

As shown in Table 4, Yoon and the present study had the largest difference of 14% in discharge coefficients. This may be due to difference in geometries, such as Yoon vertex tips not being 90 degrees and instead having a radius. Banchhor's research coincides closely with the present studies data having only a difference of 2.58%. Banchhor's study was also conducted using CFD simulations for varying H/D and vertex tip radii's. Most of their research focused on wedge meters that had a tip radius of 3 mm, where the results varied greatly from the present studies tip radius of 0 mm.

Britton and Stark conducted a physical study of how the C of sharp edged orifice meters varied with Reynolds numbers (Britton and Stark, 1986). One of the orifices that they studied had a beta value of 0.5322, which was similar to the present study's beta of 0.50. Miller has also published work for differing beta values including 0.50 as shown in Fig. 18 below (Miller, 1996).

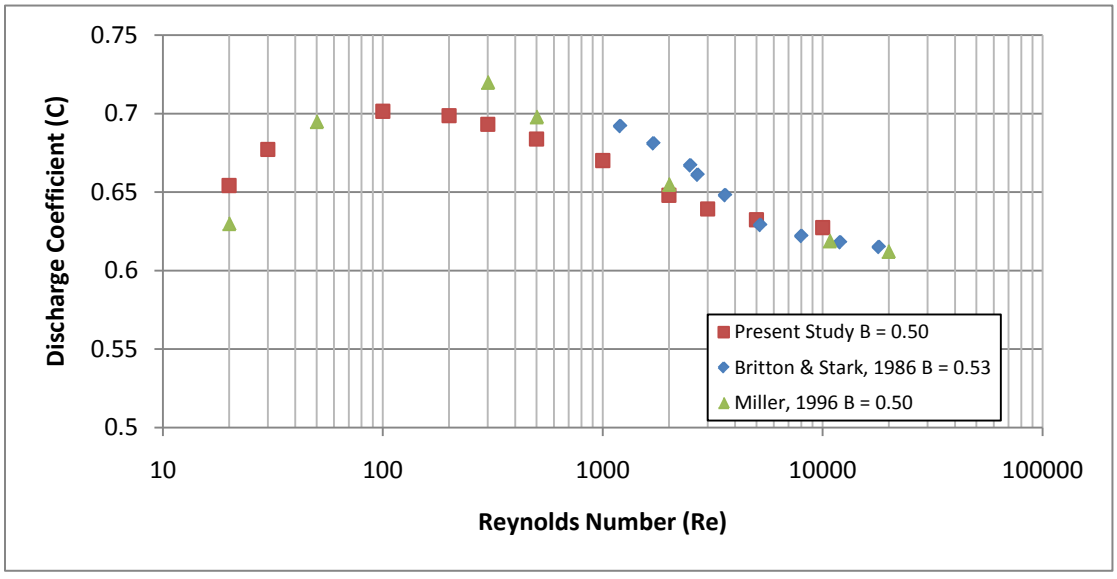

Fig. 18. Orifice plate flow meter data.

As shown in Fig. 18, all of the data series demonstrate similar trends for varying Re numbers. The maximum difference between any of the different data sets is just over 4%, which further compliments the results of the present study. Britton and Starks research focus on Re between 1,000 and 20,000, while the other two studies had a much wider range. Unlike any of the other flow meters in this study, the orifice plate does not have a constant C over any large Re range. Orifice plate flow meters are often not ideal for some measurement operations where Reynolds numbers are not known since there is no constant C, but they are usually one of the most cost efficient meters. The hump like shape at the smaller end of Re numbers is likely attributed to the unique relationship between the geometry of the orifice plate and the incoming velocity profile.

Each of the flow meters responds differently to similar flow, because of geometrical differences. In Fig. 19, the static pressure distribution across each of the flow meters is shown for heavy oil flow and similar beta values.

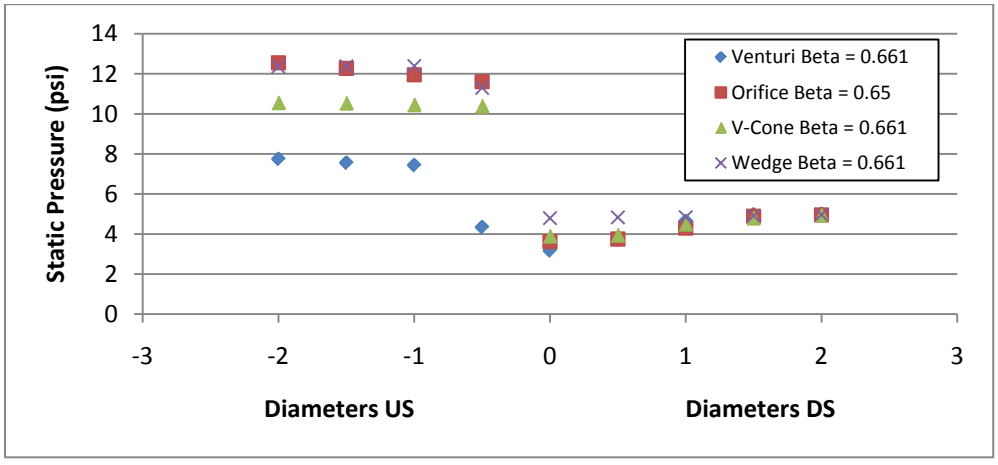

Fig. 19. Comparison of static pressure distribution at Re = 2000 through 8 in. diameter.

The orifice flow meter had the largest pressure differential across the meter while the Venturi had the smallest pressure differential. With similar beta values, diameters, viscosities, and Reynolds numbers the only variables in Fig. 19 were the discharge coefficients and pressure differentials. Therefore, meters with coefficients nearer to 1 such as the Venturi had the smallest pressure differential while the orifice plate had the lowest discharge coefficient of 0.685. The larger pressure variations are easier to determine more exact differentials with less error than extremely small pressure differences. The steep large drop in static pressure for the orifice flow meter is similar to the pressure distribution pattern presented in Bandyopadhyay's study (Bandyopadhyay and Das, 2007).

CHAPTER V

CONCLUSION

The CFD program FLUENT© was used to create multiple models in an effort to understand trends in the discharge coefficients for differential pressure flow meters with varying Reynolds numbers. The research established the discharge coefficient for Re numbers ranging from 1 to 50,000,000. For turbulent flow regimes water was modeled as the flowing fluid, while for laminar flow ranges heavy oil was modeled to create larger viscosities resulting in smaller Re. Various models were generated for each of the flow meters being analyzed to determine effects of pipe size and beta values on the discharge coefficient.

Users must keep in mind that since only a few common beta ratios were tested for each of the meters, there may be a variation of results when using beta ratios found outside of the study range. The Venturi, V-cone and wedge flow meters all have relative constant discharge coefficients for common Reynolds numbers, but with the additional information found in this study nearly all types of flows can be determined. The physical data range was small in comparison to the numerical flow range for each of the test simulations. The accuracy of the numerical results should be greatest at Reynolds numbers of less than 2300, because turbulence models were not needed in this region therefore increasing the accuracy of the results. The use of Computational Fluid Dynamics aids in the ability to replicate this study while minimizing human errors. The data from this study demonstrates that with possible discharge coefficients near 0.20 for some of the flow meters that the iterative process be used to minimize flow rate errors.

Four different graphs were developed to present the results of the research, with one graph for each of the flow meters being studied. These graphs can be used by readers to determine how each meter's performance may be characterized for pipeline flows for varying viscosities of non-compressible fluids. The results from this study could be expanded with future research of flow meter discharge coefficients for additional differential producing meters.

One area of particular interest is the possibility of using boundary layers on the model walls when generating the model mesh. Performing this research will help to ensure the accuracy of using the enhanced near-wall treatment option for the k-epsilon model for turbulent flows, rather than the standard wall treatment as used in this study. Another area of potential interest is performing tests over a wide range of beta values to obtain a more complete understanding of discharge coefficient relationships.

References

Ashrafixadeh, S.N., Kamran, M., 2010. Emulsification of heavy crude oil in water for pipeline transportation. J. Pet. Sci. Eng., 71:3, 205-211.

Banchhor, P., Singh, S., Seshadri, V., Gandhi, B., 2002. Performance charateristics of wedge flowmeters using CFD. J. Comput. Fluid Dyn., 11:3, 279-284.

Bandyopadhyay, T.K., Das, S.K., 2007. Non-newtonian pseudoplastic liquid flow through small diameter piping components. J. Pet. Sci. Eng., 55, 156-166.

Britton, C.. Stark, S., 1986. New data for the quadrant edge orifice, CEESI, Nunn, Colorado. http://www.ceesi.com/docs_library/publications/12_New_Data_ Quadrant _Edged_Orifice.pdf (accessed Feb. 23, 2010).

Clark, P., Pilehvari, A., 1993. Characterization of crude oil-in-water emulsions. J. Pet. Sci. Eng., 9, 165-181.

Celik, I., Ghia, U., Roache, P., Freitas, C., 2008. Procedure for estimation and reporting of uncertainty due to discretisation in CFD applications. J. Fluids Eng., 130:7, 1-4.

Fluent Inc. 2003. 24.2 Discretisation, ANSYS fluent, Canonsburg, Pennsylvania. http://jullio.pe.kr/Fluent6.1/help/html/ug/node814.htm (accessed Sept 29,2010).

Fluent Inc. 2006. 25.3.1 Spatial discretisation, ANSYS fluent, Canonsburg, Pennsylvania. http://my.fit.edu/itresources/manuals/Fluent6.3/help/html/ug/ node992.htm (accessed Aug. 23, 2010).

GOA (Government of Alberta), 2009. Energy-facts and statistics, GOA, Alberta, Canada. http://www.energy.alberta.ca/OilSands/791.asp (accessed Feb. 18, 2010).

McCrometer, 2002. Flow calculations for the V-cone and wafer-cone flow meters, McCrometer, Hemet, California. http://www.iceweb.com.au/Flow/V-Cone/V-Cone _Flow_Calculations.pdf (accessed Feb. 10, 2010).

Miller, G., Pinguet, B., Theuveny, B., Mosknes, P., 2009. The influence of liquid viscosity on multiphase flow meters, TUV NEL, Glasgow, United Kingdom. http://www.tekna.no/ikbViewer/Content/778329/14_Miller%20HV_Multiphase.pdf (accessed Feb. 16, 2010).

Miller, R. W., 1996. Flow Measurement Engineering Handbook, third ed. McGraw-Hill Companies, Inc., Boston, MA.

NASA (National Aeronautics and Space Administration), 2008. Navier-Stokes equations, NASA, Washington, D.C. http://www.grc.nasa.gov/ WWW/K-12/airplane/nseqs.html (accessed Aug. 24, 2010).

PSFI (Primary Signal Flow Inc.), 2001. SCFP-wedge type flow meter, PSFI, Warwick, Rhode Island. http://www.pfsflowproducts.com/wedgetyp.htm (accessed Feb. 12, 2010).

Singh, S., Seshadri, V., Singh, R., Gawhade R., 2006. Effect of upstream flow disturbances on the performance characteristics of a V-cone flow meter. J. Flow Meas. Instrum., 17:5, 291-297.

Tan, C., Dong, F., Zhang, F., Li, W., 2009. Oil-water two-phase flow measurement with a V-cone meter in a horizontal pipe. International Instrumentation and Measurement Technology Conference., Tianjin, China.

Versteeg, H. K., Malalasekera W., 2007. An Introduction to Computational Fluid Dynamics- The Finite Volume Method, second ed., Pearson Education Limited, Harlow England.

Yoon, J., Sung, N., Lee, C., 2007. Discharge coefficient equation of a segmental wedge flow meter. J. Process Mech. Eng., 222:E, 79-83.

APPENDICES

APPENDIX A: MODEL IMAGES

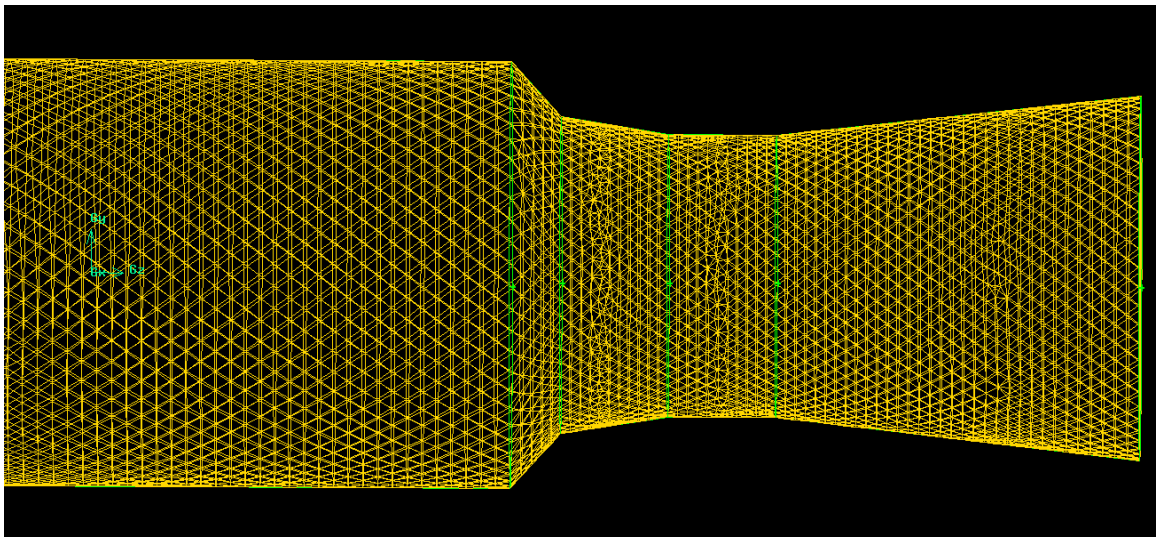

Fig. A1. Mesh of Venturi meter.

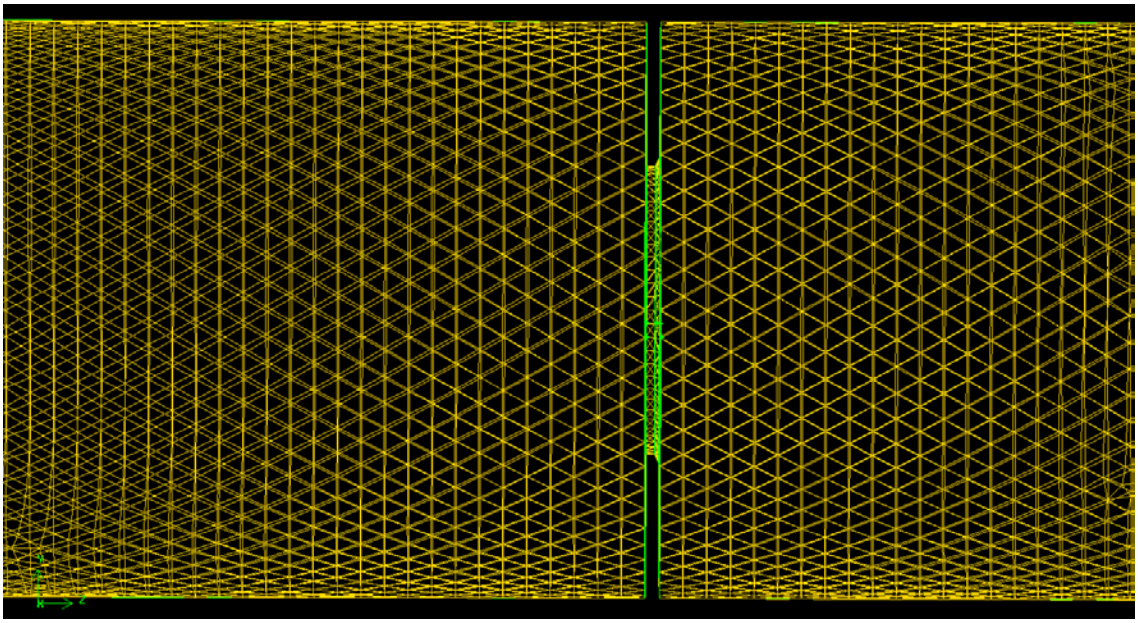

Fig. A2. Mesh of orifice plate.

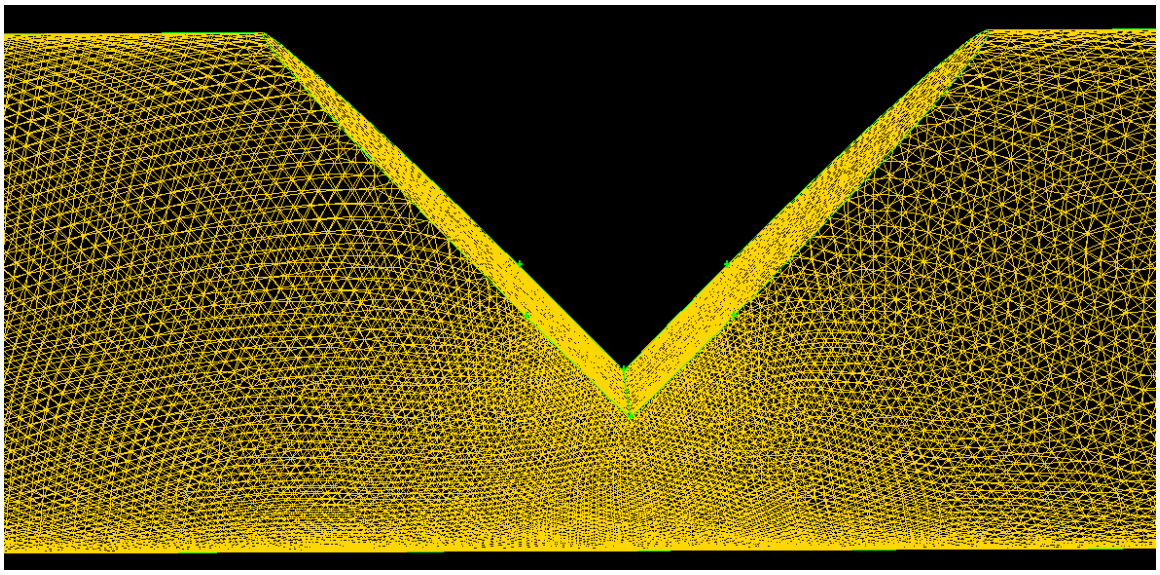

Fig. A3. Wedge mesh.

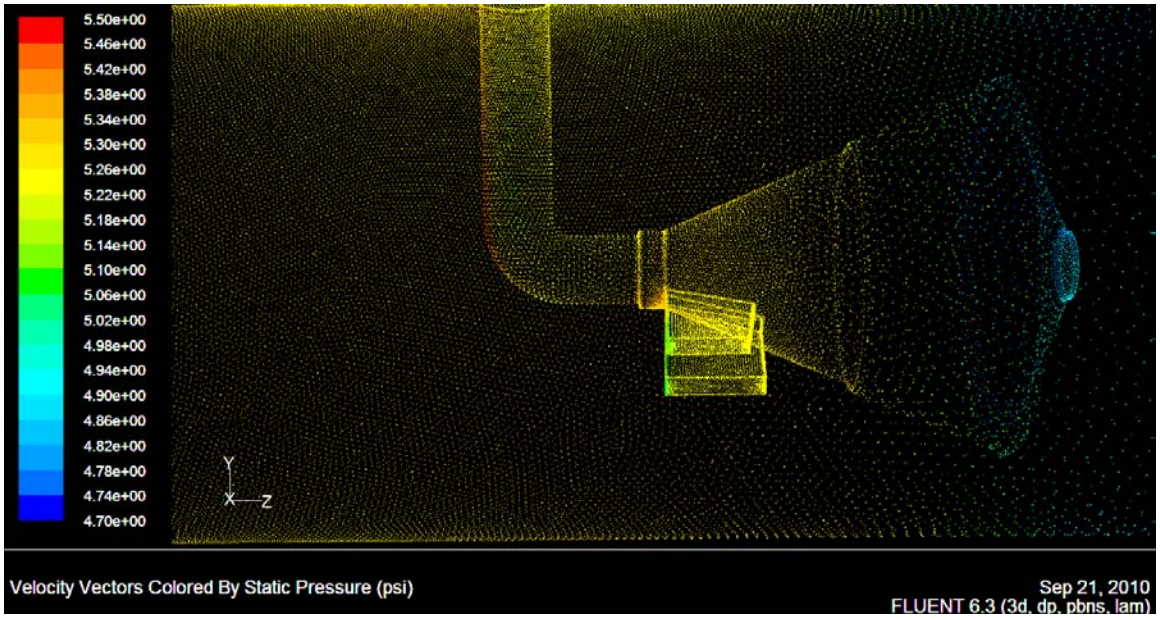

Fig. A4. Pressure on a V-cone model.

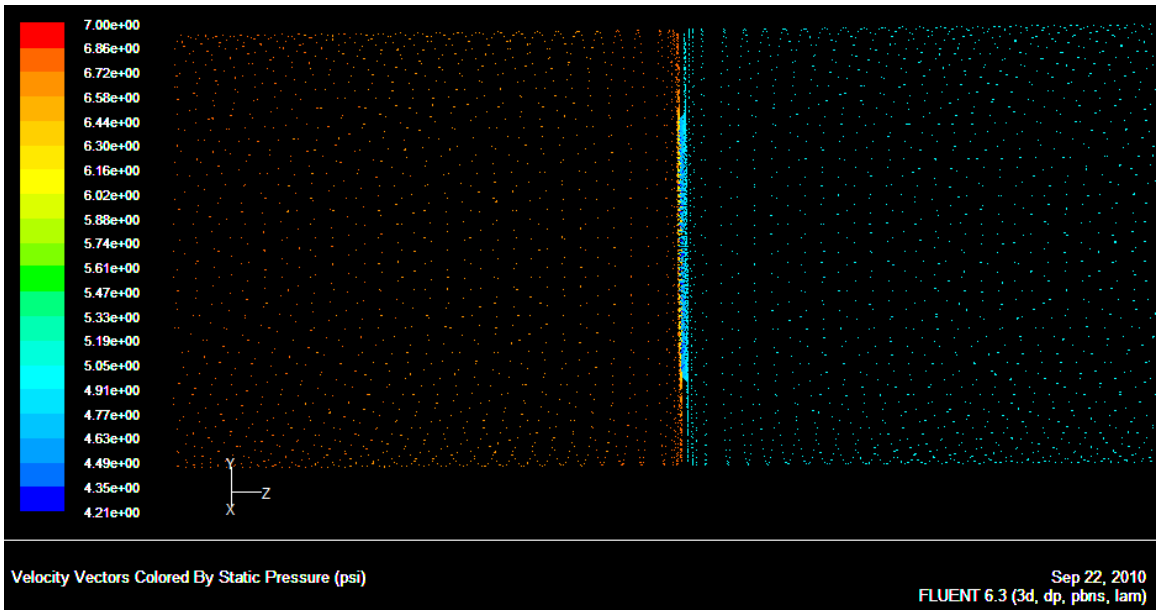

Fig. A5. Standard concentric orifice plate pressure vectors.

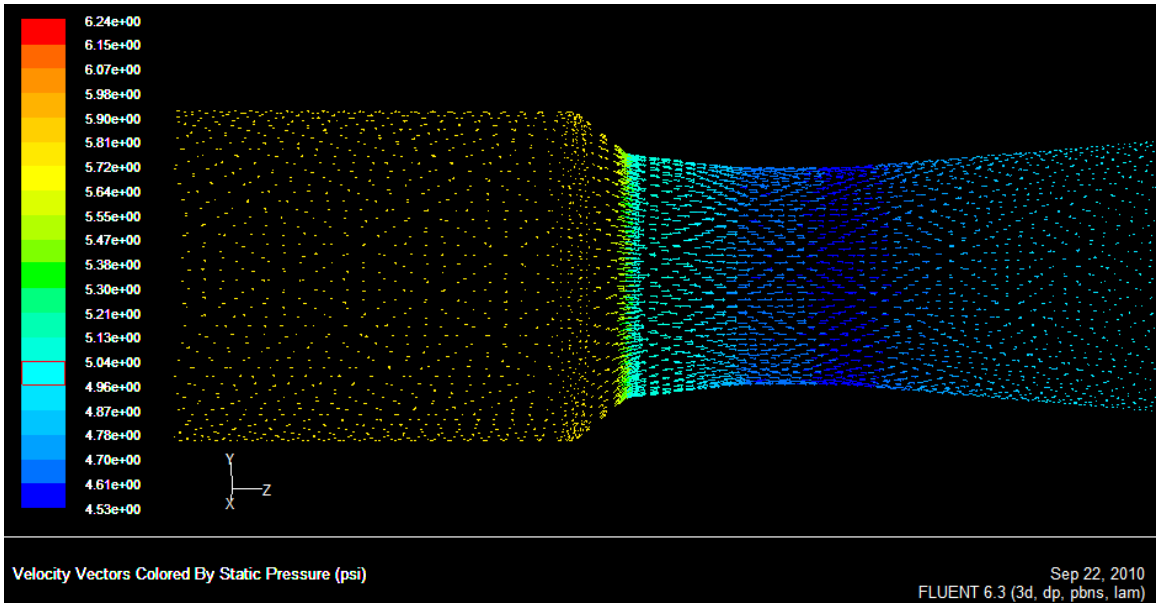

Fig. A6. Venturi flow meter pressure vectors.

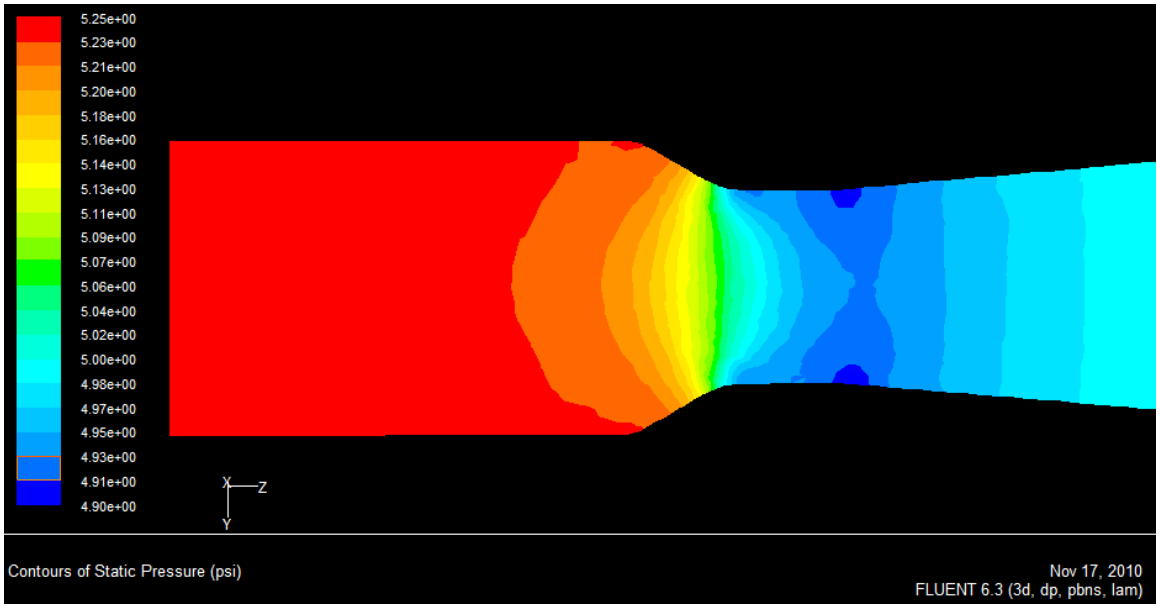

Fig. A7. Centerline Venturi pressure contours.

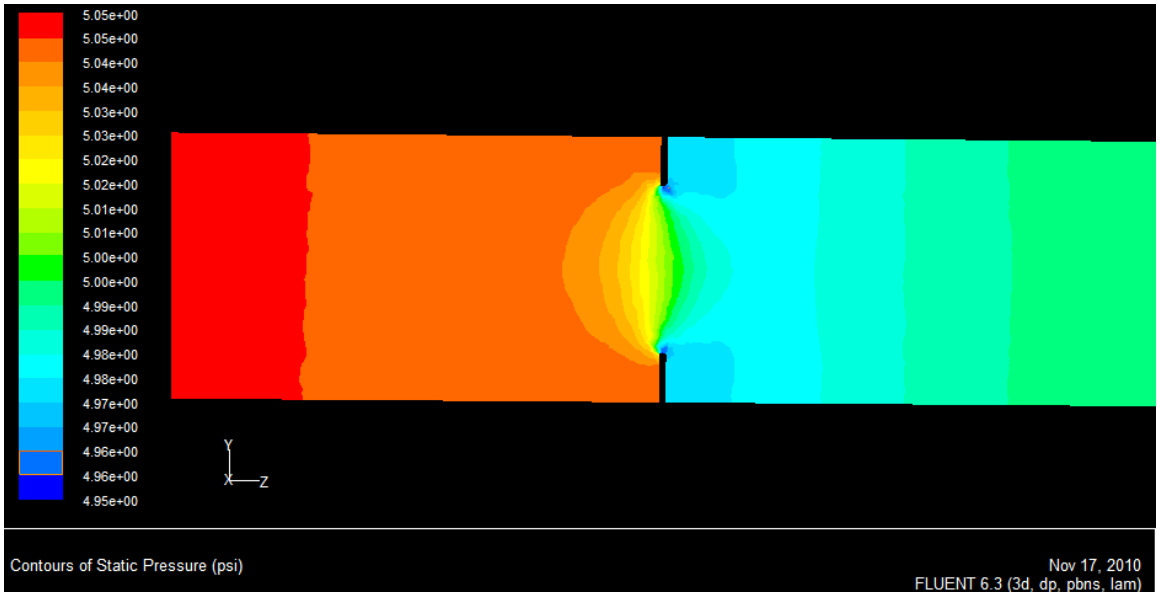

Fig. A8. Centerline orifice plate pressure contours.

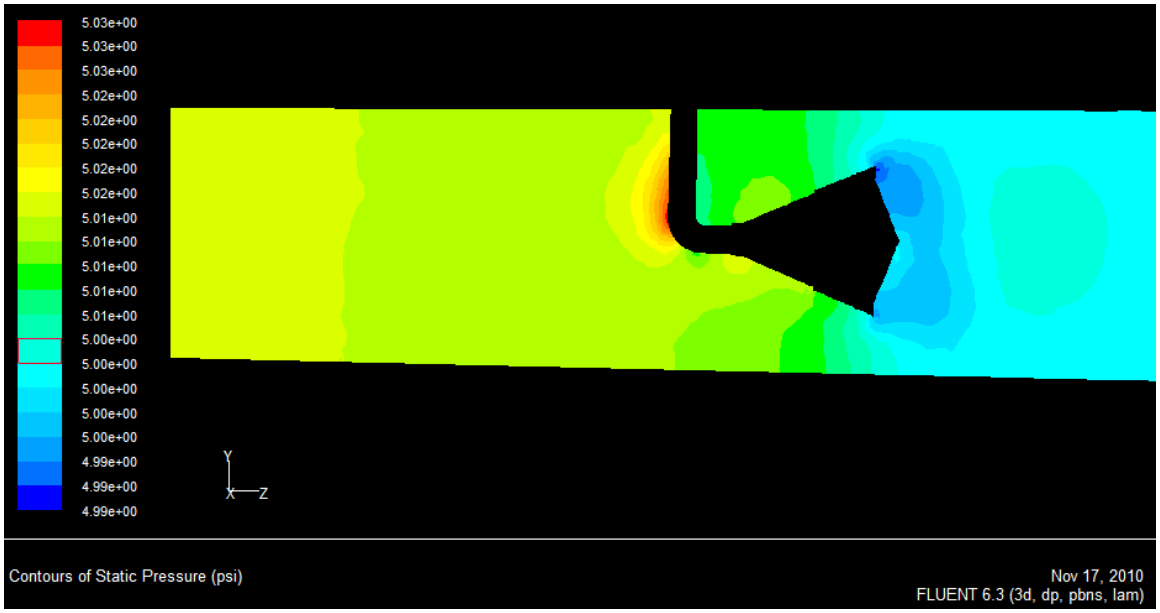

Fig. A9. Centerline V-cone pressure contours.

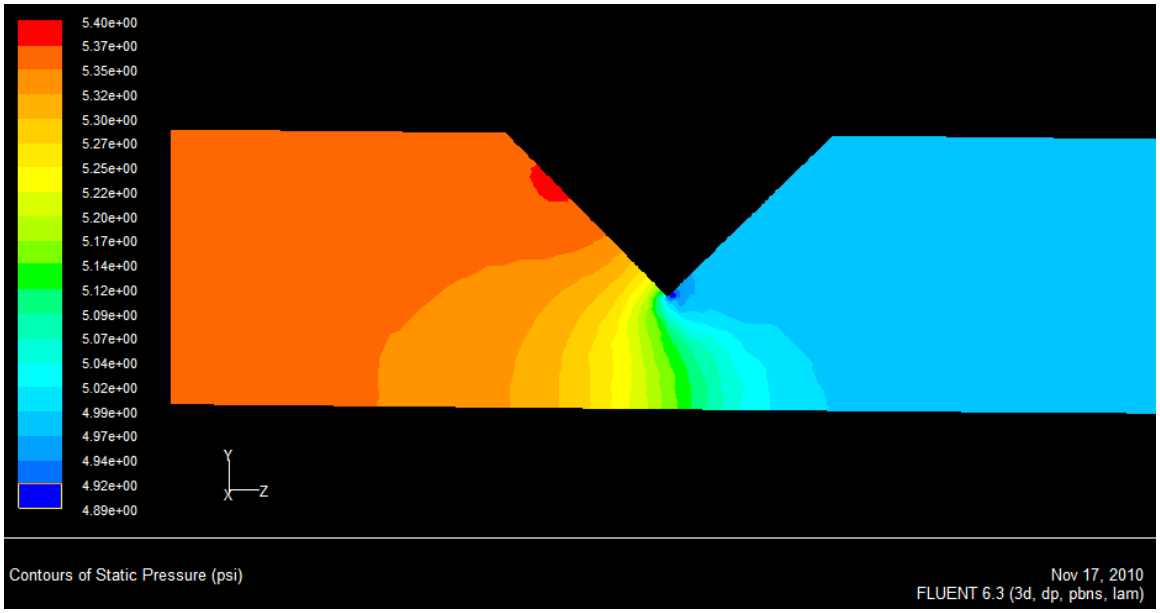

Fig. A10. Centerline wedge pressure contours.

APPENDIX B: DISCHARGE COEFFICIENT TABLES

Data for 12 inch Sharp Venturi

Date	6/7/2010	
D1 =	6.065	in
D2 =	4.009	in
Density =	62.43	lb/ft^3
Gravity =	32.174	ft/s^2
Beta =	0.661	

Viscosity Model	Fluid	Re	Flow (gpm)	Viscosity ft^2/s	Velocity ft/s	High Tap (psi)	Low Tap (psi)	Delta H (in of H2O)	C
k-epsilon	Water	50000000	148830.20	1.67E-05	1652.80	19600.00	-59920.00	2202092.31	0.967
k-epsilon	Water	10000000	29766.03	1.67E-05	330.56	938.00	-2395.00	92298.46	0.967
k-epsilon	Water	1000000	2976.60	1.67E-05	33.06	14.75	-18.65	924.95	0.967
k-epsilon	Water	100000	297.66	1.67E-05	3.31	5.11	4.77	9.28	0.965
k-epsilon	Water	75000	223.25	1.67E-05	2.48	5.06	4.87	5.24	0.963
k-epsilon	Water	50000	148.83	1.67E-05	1.65	5.03	4.94	2.33	0.962
k-epsilon	Water	30000	89.30	1.67E-05	0.99	5.01	4.98	0.84	0.959
k-epsilon	Oil	10000	5156.89	2.89E-03	57.27	46.90	-56.30	2857.85	0.952
k-epsilon	Oil	5000	2578.44	2.89E-03	28.63	17.29	-9.10	730.80	0.944
k-epsilon	Oil	3000	1547.07	2.89E-03	17.18	10.09	0.50	265.57	0.937
k-epsilon	Oil	2000	1031.38	2.89E-03	11.45	7.53	3.17	120.74	0.930
Laminar	Oil	1000	515.69	2.89E-03	5.73	5.24	4.94	8.31	0.914
Laminar	Oil	500	257.84	2.89E-03	2.86	5.39	4.96	11.87	0.883
Laminar	Oil	300	154.71	2.89E-03	1.72	5.11	4.99	3.30	0.841
Laminar	Oil	200	103.14	2.89E-03	1.15	5.0568	4.9985	1.61	0.801
Laminar	Oil	100	51.57	2.89E-03	0.57	5.0202	5.0019	0.51	0.715
Laminar	Oil	80	41.26	2.89E-03	0.46	5.0147	5.0020	0.35	0.688
Laminar	Oil	60	30.94	2.89E-03	0.34	5.0098	5.0018	0.22	0.650
Laminar	Oil	40	20.63	2.89E-03	0.23	5.0057	5.0015	0.12	0.596
Laminar	Oil	30	15.47	2.89E-03	0.17	5.0040	5.0012	0.08	0.554
Laminar	Oil	20	10.31	2.89E-03	0.11	5.0024	5.0009	0.04	0.498
Laminar	Oil	10	5.16	2.89E-03	0.06	5.00112	5.00054	0.02	0.401
Laminar	Oil	5	2.58	2.89E-03	0.03	5.00055	5.00029	0.01	0.300
Laminar	Oil	1	0.52	2.89E-03	0.01	5.00011	5.00006	0.003	0.146

Data for 12 inch Smooth Venturi

Date	6/14/2010	
D1 =	6.065	in
D2 =	4.009	in
Density =	62.43	lb/ft^3
Gravity =	32.174	ft/s^2
Beta =	0.661	

Viscosity Model	Fluid	Re	Flow (gpm)	Viscosity ft^2/s	Velocity ft/s	High Tap (psi)	Low Tap (psi)	Delta H (in of H2O)	C
k-epsilon	Water	50000000	146193.3	1.64E-05	1623.51	19373.00	-59820.00	2193037	0.975
k-epsilon	Water	10000000	29238.66	1.64E-05	324.70	794.00	-2375.00	87756.92	0.974
k-epsilon	Water	1000000	2923.87	1.64E-05	32.47	13.31	-18.45	879.59	0.967
k-epsilon	Water	100000	292.39	1.64E-05	3.25	5.09	4.77	8.84	0.965
k-epsilon	Water	75000	219.29	1.64E-05	2.44	5.05	4.87	4.98	0.963
k-epsilon	Water	50000	146.19	1.64E-05	1.62	5.02	4.94	2.23	0.962
k-epsilon	Water	30000	87.72	1.64E-05	0.97	5.01	4.98	0.80	0.959
k-epsilon	Oil	10000	5156.89	2.89E-03	57.27	42.90	-58.50	2808.00	0.952
k-epsilon	Oil	5000	2578.44	2.89E-03	28.63	16.40	-9.30	711.69	0.944
k-epsilon	Oil	3000	1547.07	2.89E-03	17.18	9.79	0.33	261.97	0.937
k-epsilon	Oil	2000	1031.38	2.89E-03	11.45	7.42	3.07	120.43	0.930
Laminar	Oil	1000	515.69	2.89E-03	5.73	5.73	4.63	30.54	0.914
Laminar	Oil	500	257.84	2.89E-03	2.86	5.23	4.93	8.35	0.883
Laminar	Oil	300	154.71	2.89E-03	1.72	5.10	4.98	3.30	0.841
Laminar	Oil	200	103.14	2.89E-03	1.15	5.0542	4.9962	1.61	0.801
Laminar	Oil	100	51.57	2.89E-03	0.57	5.0191	5.0014	0.49	0.715
Laminar	Oil	80	41.26	2.89E-03	0.46	5.0138	5.0018	0.33	0.688
Laminar	Oil	60	30.94	2.89E-03	0.34	5.0092	5.0019	0.20	0.650
Laminar	Oil	40	20.63	2.89E-03	0.23	5.0053	5.0015	0.11	0.596
Laminar	Oil	30	15.47	2.89E-03	0.17	5.0037	5.0012	0.07	0.554
Laminar	Oil	20	10.31	2.89E-03	0.11	5.0023	5.0009	0.04	0.498
Laminar	Oil	10	5.16	2.89E-03	0.06	5.00104	5.00054	0.01	0.401
Laminar	Oil	5	2.58	2.89E-03	0.03	5.00050	5.00029	0.01	0.300
Laminar	Oil	1	0.52	2.89E-03	0.01	5.00010	5.00006	0.003	0.146

Data for 6 inch Standard Orifice Plate

Date	6/15/2010	
D1 =	6.065	in
D2 =	3.0325	in
Density =	62.43	lb/ft^3
Gravity =	32.174	ft/s^2
Beta =	0.5	

Viscosity Model	Fluid	Re	Flow (gpm)	Viscosity ft^2/s	Velocity ft/s	High Tap (psi)	Low Tap (psi)	Delta H (in of H2O)	C
k-epsilon	Water	50000000	1255546.7	1.41E-05	1394.23	512825.00	-13400	14572384.6	0.611
k-epsilon	Water	10000000	25109.35	1.41E-05	278.85	20140.00	-728.00	577883.08	0.614
k-epsilon	Water	1000000	2510.93	1.41E-05	27.88	202.41	-5.05	5744.99	0.615
k-epsilon	Water	100000	251.09	1.41E-05	2.79	6.94	4.89	56.82	0.619
k-epsilon	Oil	10000	5156.89	2.89E-03	57.27	768.60	-73.10	23308.62	0.627
k-epsilon	Oil	5000	2578.44	2.89E-03	28.63	181.86	-25.21	5734.25	0.632
k-epsilon	Oil	3000	1547.07	2.89E-03	17.18	63.61	-9.35	2020.38	0.639
Laminar	Oil	2000	1031.38	2.89E-03	11.45	35.18	4.59	847.00	0.648
Laminar	Oil	1000	515.69	2.89E-03	5.73	12.22	4.84	204.34	0.670
Laminar	Oil	500	257.84	2.89E-03	2.86	6.71	4.93	49.07	0.684
Laminar	Oil	300	154.71	2.89E-03	1.72	5.58	4.96	17.19	0.693
Laminar	Oil	200	103.14	2.89E-03	1.15	5.25	4.98	7.52	0.699
Laminar	Oil	100	51.57	2.89E-03	0.57	5.06	4.99	1.86	0.702
Laminar	Oil	80	41.26	2.89E-03	0.46	5.04	4.99	1.20	0.700
Laminar	Oil	60	30.94	2.89E-03	0.34	5.0196	4.9951	0.68	0.697
Laminar	Oil	40	20.63	2.89E-03	0.23	5.0088	4.9976	0.31	0.688
Laminar	Oil	30	15.47	2.89E-03	0.17	5.0051	4.9986	0.18	0.677
Laminar	Oil	20	10.31	2.89E-03	0.11	5.0026	4.9995	0.09	0.654
Laminar	Oil	10	5.16	2.89E-03	0.06	5.00097	5.00000	0.03	0.585
Laminar	Oil	5	2.58	2.89E-03	0.03	5.00042	5.00006	0.01	0.478
Laminar	Oil	1	0.52	2.89E-03	0.01	5.000079	5.000018	0.004	0.233

Data for 8 inch Standard Orifice Plate

Date	6/3/2010	
D1 =	7.981	in
D2 =	4.7886	in
Density =	62.43	lb/ft^3
Gravity =	32.174	ft/s^2
Beta =	0.6	

Viscosity Model	Fluid	Re	Flow (gpm)	Viscosity ft^2/s	Velocity ft/s	High Tap (psi)	Low Tap (psi)	Delta H (in of H2O)	C
k-epsilon	Water	50000000	165208.3	1.41E-05	1059.52	136560	-7250	3982430.77	0.595
k-epsilon	Water	10000000	33041.67	1.41E-05	211.90	5245.00	-357.00	155132.31	0.602
k-epsilon	Water -	1000000	3304.17	1.41E-05	21.19	56.59	1.06	1537.75	0.605
k-epsilon	Water -	100000	330.42	1.41E-05	2.12	5.50	4.95	15.11	0.610
k-epsilon	Oil	10000	6786.01	2.89E-03	43.52	193.50	-26.80	6100.62	0.624
k-epsilon	Oil	5000	3393.00	2.89E-03	21.76	47.35	-6.12	1480.71	0.633
k-epsilon	Oil	3000	2035.80	2.89E-03	13.06	18.94	0.25	517.57	0.642
Laminar	Oil	2000	1357.20	2.89E-03	8.70	10.84	2.69	225.55	0.658
Laminar	Oil	1000	678.60	2.89E-03	4.35	6.72	4.91	50.10	0.688
Laminar	Oil	500	339.30	2.89E-03	2.18	5.39	4.96	11.87	0.707
Laminar	Oil	300	203.58	2.89E-03	1.31	5.13	4.98	4.13	0.719
Laminar	Oil	200	135.72	2.89E-03	0.87	5.05	4.99	1.81	0.725
Laminar	Oil	100	67.86	2.89E-03	0.44	5.0122	4.9960	0.45	0.727
Laminar	Oil	80	54.29	2.89E-03	0.35	5.0077	4.9973	0.29	0.725
Laminar	Oil	60	40.72	2.89E-03	0.26	5.0043	4.9984	0.16	0.721
Laminar	Oil	40	27.14	2.89E-03	0.17	5.0021	4.9993	0.08	0.707
Laminar	Oil	30	20.36	2.89E-03	0.13	5.0013	4.9997	0.04	0.689
Laminar	Oil	20	13.57	2.89E-03	0.09	5.00069	4.99990	0.02	0.657
Laminar	Oil	10	6.79	2.89E-03	0.04	5.00029	5.00002	0.01	0.568
Laminar	Oil	5	3.39	2.89E-03	0.02	5.00013	5.00003	0.003	0.448
Laminar	Oil	1	0.68	2.89E-03	0.004	5.000027	5.000008	0.001	0.212

Data for 6 inch Standard Orifice Plate

Date	7/19/2010	
D1 =	6.065	in
D2 =	3.94225	in
Density =	62.43	lb/ft^3
Gravity =	32.174	ft/s^2
Beta =	0.65	

Viscosity Model	Fluid	Re	Flow (gpm)	Viscosity ft^2/s	Velocity ft/s	High Tap (psi)	Low Tap (psi)	Delta H (in of H2O)	C
k-epsilon	Water	50000000	125546.7	1.41E-05	1394.227	141250	-22250.00	4527692.31	0.607
k-epsilon	Water	10000000	25109.35	1.41E-05	278.85	5223.00	-1262.00	179584.62	0.610
k-epsilon	Water	1000000	2510.93	1.41E-05	27.88	54.81	-9.53	1781.61	0.612
k-epsilon	Water	100000	251.09	1.41E-05	2.79	5.48	4.86	17.28	0.622
k-epsilon	Oil	10000	5156.89	2.89E-03	57.27	170.90	-76.20	6842.77	0.641
k-epsilon	Oil	5000	2578.44	2.89E-03	28.63	41.41	-17.72	1637.45	0.656
k-epsilon	Oil	3000	1547.07	2.89E-03	17.18	17.09	-3.52	570.79	0.666
Laminar	Oil	2000	1031.38	2.89E-03	11.45	11.94	3.94	221.59	0.685
Laminar	Oil	1000	515.69	2.89E-03	5.73	6.62	4.74	51.97	0.736
Laminar	Oil	500	257.84	2.89E-03	2.86	5.35	4.90	12.33	0.755
Laminar	Oil	300	154.71	2.89E-03	1.72	5.11	4.96	4.35	0.763
Laminar	Oil	200	103.14	2.89E-03	1.15	5.05	4.98	1.93	0.764
Laminar	Oil	100	51.57	2.89E-03	0.57	5.01	4.99	0.50	0.754
Laminar	Oil	80	41.26	2.89E-03	0.46	5.0082	4.9966	0.32	0.748
Laminar	Oil	60	30.94	2.89E-03	0.34	5.0051	4.9984	0.19	0.738
Laminar	Oil	40	20.63	2.89E-03	0.23	5.0028	4.9996	0.09	0.715
Laminar	Oil	30	15.47	2.89E-03	0.17	5.0019	5.0000	0.05	0.692
Laminar	Oil	20	10.31	2.89E-03	0.11	5.0012	5.0002	0.03	0.648
Laminar	Oil	10	5.16	2.89E-03	0.06	5.00053	5.00019	0.01	0.546
Laminar	Oil	5	2.58	2.89E-03	0.03	5.00026	5.00012	0.004	0.425
Laminar	Oil	1	0.52	2.89E-03	0.01	5.000051	5.000026	0.001	0.202

Data for 6 inch Standard Orifice Plate

Date	6/10/2010	
D1 =	6.065	in
D2 =	4.2455	in
Density =	62.43	lb/ft^3
Gravity =	32.174	ft/s^2
Beta =	0.7	

Viscosity Model	Fluid	Re	Flow (gpm)	Viscosity ft^2/s	Velocity ft/s	High Tap (psi)	Low Tap (psi)	Delta H (in of H2O)	C
k-epsilon	Water	50000000	125546.7	1.41E-05	1394.23	88630.00	-24850.00	3142523.08	0.604
k-epsilon	Water	10000000	25109.35	1.41E-05	278.85	2986.00	-1515.00	124643.08	0.607
k-epsilon	Water	1000000	2510.93	1.41E-05	27.88	31.90	-11.79	1209.77	0.616
k-epsilon	Water	100000	251.09	1.41E-05	2.79	5.26	4.83	11.82	0.623
k-epsilon	Oil	10000	5156.89	2.89E-03	57.27	97.70	-69.70	4635.69	0.646
k-epsilon	Oil	5000	2578.44	2.89E-03	28.63	26.19	-14.04	1114.06	0.659
k-epsilon	Oil	3000	1547.07	2.89E-03	17.18	12.20	-1.80	387.58	0.670
Laminar	Oil	2000	1031.38	2.89E-03	11.45	9.25	4.11	142.17	0.700
Laminar	Oil	1000	515.69	2.89E-03	5.73	5.90	4.70	33.11	0.765
Laminar	Oil	500	257.84	2.89E-03	2.86	5.19	4.91	7.80	0.788
Laminar	Oil	300	154.71	2.89E-03	1.72	5.06	4.96	2.75	0.796
Laminar	Oil	200	103.14	2.89E-03	1.15	5.03	4.98	1.23	0.795
Laminar	Oil	100	51.57	2.89E-03	0.57	5.0081	4.9966	0.32	0.781
Laminar	Oil	80	41.26	2.89E-03	0.46	5.0057	4.9982	0.21	0.772
Laminar	Oil	60	30.94	2.89E-03	0.34	5.0038	4.9994	0.12	0.756
Laminar	Oil	40	20.63	2.89E-03	0.23	5.0022	5.0001	0.06	0.726
Laminar	Oil	30	15.47	2.89E-03	0.17	5.0016	5.0003	0.04	0.696
Laminar	Oil	20	10.31	2.89E-03	0.11	5.00097	5.00030	0.02	0.644
Laminar	Oil	10	5.16	2.89E-03	0.06	5.00046	5.00021	0.01	0.532
Laminar	Oil	5	2.58	2.89E-03	0.03	5.00023	5.00012	0.008	0.407
Laminar	Oil	1	0.52	2.89E-03	0.01	5.000045	5.000026	0.007	0.191

Data for 10 inch V-Cone

Date	7/8/2010	
D1 =	10.137	in
D2 =	7.244	in
Density =	62.43	lb/ft^3
Gravity =	32.174	ft/s^2
Beta =	0.6995	

Viscosity Model	Fluid	Re	Flow (gpm)	Viscosity ft^2/s	Velocity ft/s	High Tap (psi)	Low Tap (psi)	Delta H (in of H2O)	C
k-epsilon	Water	50000000	209838.9	1.41E-05	834.17	15260.00	-8818.00	666775.38	0.787
k-epsilon	Water	10000000	41967.59	1.41E-05	166.83	572.50	-382.00	26432.31	0.790
k-epsilon	Water	1000000	4196.76	1.41E-05	16.68	10.63	1.13	263.08	0.792
k-epsilon	Water	100000	419.68	1.41E-05	1.67	5.06	4.96	2.63	0.792
k-epsilon	Oil	30000	25353.31	2.84E-03	100.79	211.80	-144.50	9866.77	0.781
k-epsilon	Oil	20000	16902.21	2.84E-03	67.19	97.35	-63.81	4462.89	0.774
k-epsilon	Oil	10000	8451.10	2.84E-03	33.60	28.20	-12.98	1140.23	0.766
k-epsilon	Oil	7500	6338.33	2.84E-03	25.20	18.19	-5.14	646.14	0.763
k-epsilon	Oil	5000	4225.55	2.84E-03	16.80	10.98	0.43	292.18	0.757
k-epsilon	Oil	4000	3380.44	2.84E-03	13.44	8.90	2.12	187.62	0.755
k-epsilon	Oil	3000	2535.33	2.84E-03	10.08	7.26	3.40	106.98	0.750
Laminar	Oil	2000	1690.22	2.84E-03	6.72	6.08	4.32	48.63	0.742
Laminar	Oil	1000	845.11	2.84E-03	3.36	5.30	4.84	12.88	0.721
Laminar	Oil	500	422.56	2.84E-03	1.68	5.09	4.97	3.59	0.682
Laminar	Oil	300	253.53	2.84E-03	1.01	5.04	4.99	1.45	0.645
Laminar	Oil	200	169.02	2.84E-03	0.67	5.0222	4.9966	0.71	0.615
Laminar	Oil	150	126.77	2.84E-03	0.50	5.0146	4.9986	0.44	0.584
Laminar	Oil	100	84.51	2.84E-03	0.34	5.0084	4.9999	0.24	0.533
Laminar	Oil	80	67.61	2.84E-03	0.27	5.0067	5.0001	0.18	0.502
Laminar	Oil	60	50.71	2.84E-03	0.20	5.0044	5.0002	0.11	0.458
Laminar	Oil	40	33.80	2.84E-03	0.13	5.0027	5.0002	0.07	0.394
Laminar	Oil	30	25.35	2.84E-03	0.10	5.0019	5.0002	0.05	0.350
Laminar	Oil	20	16.90	2.84E-03	0.07	5.0012	5.0001	0.03	0.292
Laminar	Oil	10	8.45	2.84E-03	0.03	5.00059	5.00004	0.02	0.210
Laminar	Oil	5	4.23	2.84E-03	0.02	5.00029	5.00002	0.01	0.150
Laminar	Oil	1	0.85	2.84E-03	0.003	5.000057	5.000003	0.002	0.067

Data for 12 inch V-Cone

Date	7/15/2010	
D1 =	12.075	in
D2 =	9.06	in
Density =	62.43	lb/ft^3
Gravity =	32.174	ft/s^2
Beta =	0.6611	

Viscosity Model	Fluid	Re	Flow (gpm)	Viscosity ft^2/s	Velocity ft/s	High Tap (psi)	Low Tap (psi)	Delta H (in of H2O)	C
k-epsilon	Water	50000000	249954.9	1.41E-05	700.29	20830.00	-690.00	595938.46	0.802
k-epsilon	Water	10000000	49990.99	1.41E-05	140.06	747.00	-122.00	24064.62	0.805
k-epsilon	Water	1000000	4999.10	1.41E-05	14.01	12.25	3.56	240.45	0.803
k-epsilon	Water	100000	499.91	1.41E-05	1.40	5.07	4.98	2.40	0.804
k-epsilon	Oil	30000	30200.38	2.84E-03	84.61	271.40	-57.10	9096.92	0.789
k-epsilon	Oil	20000	20133.59	2.84E-03	56.41	122.82	-27.05	4150.25	0.778
k-epsilon	Oil	10000	10066.79	2.84E-03	28.20	33.78	-4.21	1052.03	0.773
k-epsilon	Oil	7500	7550.10	2.84E-03	21.15	20.89	-0.80	600.65	0.767
k-epsilon	Oil	5000	5033.40	2.84E-03	14.10	11.83	2.12	268.86	0.765
k-epsilon	Oil	4000	4026.72	2.84E-03	11.28	9.29	3.05	172.66	0.763
k-epsilon	Oil	3000	3020.04	2.84E-03	8.46	7.35	3.80	98.32	0.759
Laminar	Oil	2000	2013.36	2.84E-03	5.64	6.46	4.85	44.60	0.750
Laminar	Oil	1000	1006.68	2.84E-03	2.82	5.30	4.87	11.89	0.727
Laminar	Oil	500	503.34	2.84E-03	1.41	5.09	4.98	3.21	0.700
Laminar	Oil	300	302.00	2.84E-03	0.85	5.04	4.99	1.30	0.661
Laminar	Oil	200	201.34	2.84E-03	0.56	5.0201	4.9966	0.65	0.622
Laminar	Oil	150	151.00	2.84E-03	0.42	5.0131	4.9983	0.41	0.588
Laminar	Oil	100	100.67	2.84E-03	0.28	5.0074	4.9995	0.22	0.537
Laminar	Oil	80	80.53	2.84E-03	0.23	5.0055	4.9999	0.16	0.506
Laminar	Oil	60	60.40	2.84E-03	0.17	5.0038	5.0000	0.11	0.462
Laminar	Oil	40	40.27	2.84E-03	0.11	5.0024	5.0001	0.06	0.396
Laminar	Oil	30	30.20	2.84E-03	0.08	5.0018	5.0001	0.05	0.349
Laminar	Oil	20	20.13	2.84E-03	0.06	5.0011	5.0001	0.03	0.289
Laminar	Oil	10	10.07	2.84E-03	0.03	5.00055	5.00002	0.01	0.207
Laminar	Oil	5	5.03	2.84E-03	0.01	5.00027	5.00001	0.01	0.147
Laminar	Oil	1	1.01	2.84E-03	0.003	5.000054	5.000001	0.001	0.066

Data for 12 inch V-Cone

Date	7/12/2010	
D1 =	12.082	in
D2 =	6.91	in
Density =	62.43	lb/ft^3
Gravity =	32.174	ft/s^2
Beta =	0.8203	

Viscosity Model	Fluid	Re	Flow (gpm)	Viscosity ft^2/s	Velocity ft/s	High Tap (psi)	Low Tap (psi)	Delta H (in of H2O)	C
k-epsilon	Water	50000000	250099.9	1.41E-05	699.88	3552.00	-3850.00	204978.5	0.734
k-epsilon	Water	10000000	50019.97	1.41E-05	139.98	136.90	-157.50	8152.62	0.741
k-epsilon	Water	1000000	5002.00	1.41E-05	14.00	6.33	3.33	82.97	0.730
k-epsilon	Water	100000	500.20	1.41E-05	1.40	5.01	4.98	0.83	0.730
k-epsilon	Oil	30000	30217.89	2.84E-03	84.56	55.84	-55.80	3091.57	0.731
k-epsilon	Oil	20000	20145.26	2.84E-03	56.37	28.06	-20.40	1341.97	0.725
k-epsilon	Oil	10000	10072.63	2.84E-03	28.19	10.97	-1.41	342.89	0.723
k-epsilon	Oil	7500	7554.47	2.84E-03	21.14	8.44	1.52	191.63	0.724
k-epsilon	Oil	5000	5036.31	2.84E-03	14.09	6.61	3.51	85.85	0.722
k-epsilon	Oil	4000	4029.05	2.84E-03	11.27	6.07	4.04	56.41	0.721
k-epsilon	Oil	3000	3021.79	2.84E-03	8.46	5.64	4.50	31.65	0.714
Laminar	Oil	2000	2014.53	2.84E-03	5.64	5.28	4.75	14.73	0.705
Laminar	Oil	1000	1007.26	2.84E-03	2.82	5.09	4.94	3.99	0.685
Laminar	Oil	500	503.63	2.84E-03	1.41	5.03	4.99	1.09	0.644
Laminar	Oil	300	302.18	2.84E-03	0.85	5.0132	4.9966	0.46	0.605
Laminar	Oil	200	201.45	2.84E-03	0.56	5.0075	4.9992	0.23	0.557
Laminar	Oil	150	151.09	2.84E-03	0.42	5.0051	4.9998	0.15	0.526
Laminar	Oil	100	100.73	2.84E-03	0.28	5.0030	5.0001	0.08	0.472
Laminar	Oil	80	80.58	2.84E-03	0.23	5.0023	5.0002	0.06	0.440
Laminar	Oil	60	60.44	2.84E-03	0.17	5.0016	5.0002	0.04	0.400
Laminar	Oil	40	40.29	2.84E-03	0.11	5.00102	5.00014	0.02	0.343
Laminar	Oil	30	30.22	2.84E-03	0.08	5.00074	5.00011	0.02	0.303
Laminar	Oil	20	20.15	2.84E-03	0.06	5.00047	5.00007	0.01	0.253
Laminar	Oil	10	10.07	2.84E-03	0.03	5.00023	5.00003	0.01	0.182
Laminar	Oil	5	5.04	2.84E-03	0.01	5.000112	5.000013	0.003	0.128
Laminar	Oil	1	1.01	2.84E-03	0.003	5.000022	5.000002	0.001	0.057

Data for 6 inch Wedge

Date	6/2/2010	
D1 =	6.065	in
D2 =	1.82	in
Density =	62.43	lb/ft^3
Gravity =	32.174	ft/s^2
Beta =	0.5023	

Viscosity Model	Fluid	Re	Flow (gpm)	Viscosity ft^2/s	Velocity ft/s	High Tap (psi)	Low Tap (psi)	Delta H (in of H2O)	C
k-epsilon	Water	50000000	125546.7	1.41E-05	1394.23	357650.00	-2420.00	9971169.23	0.732
k-epsilon	Water	10000000	25109.35	1.41E-05	278.85	14260.00	-243.50	401635.38	0.729
k-epsilon	Water	1000000	2510.93	1.41E-05	27.88	146.54	1.53	4015.80	0.729
k-epsilon	Water	100000	251.09	1.41E-05	2.79	6.39	4.94	40.05	0.730
k-epsilon	Water	5000	12.64	1.42E-05	0.14	5.00	4.99	0.24	0.727
k-epsilon	Oil	5000	2528.16	2.84E-03	28.08	145.52	-2.68	4103.86	0.726
k-epsilon	Oil	20	10.31	2.84E-03	0.11	5.00	5.00	0.12	0.556
Laminar	Oil	20	10.31	2.84E-03	0.11	5.00	5.00	0.12	0.555
Laminar	Oil	500	257.84	2.89E-03	2.86	6.51	4.97	42.84	0.725
Laminar	Oil	400	206.27	2.89E-03	2.29	5.97	4.98	27.53	0.723
Laminar	Oil	300	154.70	2.89E-03	1.72	5.55	4.98	15.58	0.721
Laminar	Oil	200	103.14	2.89E-03	1.15	5.24	4.99	7.02	0.716
Laminar	Oil	100	51.57	2.89E-03	0.57	5.0614	4.9951	1.84	0.700
Laminar	Oil	80	41.25	2.89E-03	0.46	5.0401	4.9967	1.20	0.692
Laminar	Oil	60	30.94	2.89E-03	0.34	5.0239	4.9983	0.71	0.677
Laminar	Oil	40	20.63	2.89E-03	0.23	5.0122	4.9997	0.35	0.645
Laminar	Oil	30	15.47	2.89E-03	0.17	5.0078	5.0001	0.22	0.613
Laminar	Oil	10	5.16	2.89E-03	0.06	5.00191	5.00018	0.05	0.433
Laminar	Oil	5	2.58	2.89E-03	0.03	5.00089	5.00009	0.02	0.319
Laminar	Oil	1	0.52	2.89E-03	0.01	5.000171	5.000017	0.004	0.146

Data for 8 inch Wedge

Date	6/16/2010	
D1 =	7.981	in
D2 =	3.192	in
Density =	62.43	lb/ft^3
Gravity =	32.174	ft/s^2
Beta =	0.6110	

Viscosity Model	Fluid	Re	Flow (gpm)	Viscosity ft^2/s	Velocity ft/s	High Tap (psi)	Low Tap (psi)	Delta H (in of H2O)	C
k-epsilon	Water	50000000	165208.0	1.41E-05	1059.52	92450.00	-1442.00	2600086.15	0.705
k-epsilon	Water	10000000	33041.67	1.41E-05	211.90	3641.00	-221.00	106947.69	0.695
k-epsilon	Water	1000000	3304.17	1.41E-05	21.19	41.14	2.91	1058.68	0.699
k-epsilon	Water	100000	330.42	1.41E-05	2.12	5.35	4.97	10.50	0.702
k-epsilon	Oil	5000	3326.84	2.84E-03	21.34	39.55	0.34	1085.82	0.700
Laminar	Oil	1000	665.37	2.84E-03	4.27	6.46	4.94	42.18	0.705
Laminar	Oil	500	332.68	2.84E-03	2.13	5.36	4.98	10.70	0.700
Laminar	Oil	300	199.61	2.84E-03	1.28	5.13	4.99	3.92	0.694
Laminar	Oil	200	133.07	2.84E-03	0.85	5.06	4.99	1.77	0.688
Laminar	Oil	100	66.54	2.84E-03	0.43	5.0151	4.9983	0.46	0.672
Laminar	Oil	80	53.23	2.84E-03	0.34	5.0101	4.9991	0.31	0.663
Laminar	Oil	60	39.92	2.84E-03	0.26	5.0063	4.9997	0.18	0.645
Laminar	Oil	40	26.61	2.84E-03	0.17	5.0034	5.0001	0.09	0.606
Laminar	Oil	30	19.96	2.84E-03	0.13	5.0023	5.0001	0.06	0.567
Laminar	Oil	20	13.31	2.84E-03	0.09	5.00134	5.00014	0.03	0.503
Laminar	Oil	10	6.65	2.84E-03	0.04	5.00060	5.00008	0.01	0.384
Laminar	Oil	5	3.33	2.84E-03	0.02	5.00028	5.00004	0.01	0.280
Laminar	Oil	1	0.67	2.84E-03	0.004	5.000055	5.000009	0.001	0.127

Data for 8 inch Wedge

Date	6/9/2010	
D1 =	7.981	in
D2 =	2.394	in
Density =	62.43	lb/ft^3
Gravity =	32.174	ft/s^2
Beta =	0.5023	

Viscosity Model	Fluid	Re	Flow (gpm)	Viscosity ft^2/s	Velocity ft/s	High Tap (psi)	Low Tap (psi)	Delta H (in of H2O)	C
k-epsilon	Water	50000000	165208.3	1.41E-05	1059.52	206450.00	-857.00	5740809.23	0.733
k-epsilon	Water	10000000	33041.67	1.41E-05	211.90	8252.00	-52.00	229956.92	0.732
k-epsilon	Water	1000000	3304.17	1.41E-05	21.19	87.34	4.12	2304.55	0.731
k-epsilon	Water	100000	330.42	1.41E-05	2.12	5.80	4.97	23.04	0.732
k-epsilon	Oil	5000	3326.84	2.84E-03	21.34	87.45	2.49	2352.74	0.729
Laminar	Oil	1000	665.37	2.84E-03	4.27	8.36	4.96	94.07	0.730
Laminar	Oil	500	332.68	2.84E-03	2.13	5.85	4.99	23.78	0.725
Laminar	Oil	300	199.61	2.84E-03	1.28	5.31	4.99	8.66	0.721
Laminar	Oil	200	133.07	2.84E-03	0.85	5.1365	4.9956	3.90	0.716
Laminar	Oil	100	66.54	2.84E-03	0.43	5.0350	4.9980	1.02	0.699
Laminar	Oil	80	53.23	2.84E-03	0.34	5.0228	4.9985	0.67	0.690
Laminar	Oil	60	39.92	2.84E-03	0.26	5.0135	4.9992	0.40	0.674
Laminar	Oil	40	26.61	2.84E-03	0.17	5.0068	4.9998	0.19	0.641
Laminar	Oil	30	19.96	2.84E-03	0.13	5.0044	5.0000	0.12	0.610
Laminar	Oil	20	13.31	2.84E-03	0.09	5.0025	5.0001	0.07	0.551
Laminar	Oil	10	6.65	2.84E-03	0.04	5.00105	5.00008	0.03	0.432
Laminar	Oil	5	3.33	2.84E-03	0.02	5.00049	5.00004	0.01	0.318
Laminar	Oil	1	0.67	2.84E-03	0.004	5.000094	5.000008	0.002	0.145

APPENDIX C: NUMERICAL UNCERTAINTY DATA

Venturi 1 Beta = 0.661 Numerical Error

Density	999.966	
Viscosity	0.001522	
Velocity	3.247024	
Grid # 1		
Count =	40	
Volume =	0.03526	m^3
Cells =	112045	
h1 =	0.006802	
Grid # 2		
Count =	34	
Volume =	0.03522	m^3
Cells =	54566	
h2 =	0.008643	
Grid # 3		
Count =	20	
Volume =	0.03522	m^3
Cells =	24579	
h3 =	0.011274	
r =	1.657459	
r21 =	1.270549	
r32 =	1.304522	
Theta 3 =	0.9648	
Theta 2 =	0.9711	
Theta 1 =	0.968	
e32 =	0.0063	
e21 =	0.0031	
q(p) =	-0.12471	
p =	2.440773	
s=	0.895403	
Theta ext21 =	0.964096	
Theta ext32 =	0.977998	

Approximate		
Relative Error $_{12}$=	0.320248	%
Relative Error $_{23}$=	0.648749	%
Extrapolated		
Relative Error $_{12}$=	0.404975	%
Relative Error $_{23}$=	0.705298	%
Grid Convergence Index		
GCI fine $_{12}$ =	0.504177	%
GCI fine $_{23}$=	**0.887885**	%
Maximum Error =	**0.89**	**%**

Venturi 2 Beta = 0.661 Numerical Error

Density	999.966		**Approximate**		
Viscosity	0.001555		Relative Error $_{12}$=	0.437227	%
Velocity	3.305589		Relative Error $_{23}$=	0.290216	%
	Grid # 1		**Extrapolated**		
Count =	60		Relative Error $_{12}$=	0.087443	%
Volume =	0.03539	m^3	Relative Error $_{23}$=	0.013701	%
Cells =	91684				
h1 =	0.007281				
			GCI fine $_{12}$ =	**1.099992**	%
	Grid # 2		GCI fine $_{23}$=	0.359707	%
Count =	42				
Volume =	0.03534	m^3	**Maximum Error =**	**1.10**	**%**
Cells =	55765				
h2 =	0.00859				
	Grid # 3				
Count =	35				
Volume =	0.03521	m^3			
Cells =	23577				
h3 =	0.011431				
r =	1.569862				
r21 =	1.179701				
r32 =	1.330729				
Theta 3 =	0.962				
Theta 2 =	0.9648				
Theta 1 =	0.9606				
e32 =	0.0028				
e21 =	0.0042				
q(p) =	-1.38705				
p =	10.84657				
s=	0.61837				
Theta ext21 =	0.959761				
Theta ext32 =	0.964932				

Orifice Beta = 0.70 Numerical Error

Density	999.7		**Approximate**		
Viscosity	0.001308		**Relative Error $_{12}$=**	**1.343661**	**%**
Velocity	2.788453		Relative Error $_{23}$=	0.176254	%
Grid # 1			**Extrapolated**		
Count =	60		Relative Error $_{12}$=	0.065009	%
Volume (m^3) =	0.04021	m^3	Relative Error $_{23}$=	0.002964	%
Cells =	93916				
h1 =	0.007537		**Grid Convergence Index**		
			GCI fine $_{12}$ =	0.081314	%
Grid # 2			GCI fine $_{23}$=	0.003706	%
Count =	45				
Volume =	0.04078	m^3	**Maximum Error =**	**1.40**	**%**
Cells =	43690				
h2 =	0.009773				
Grid # 3					
Count =	30				
Volume =	0.04052	m^3			
Cells =	15351				
h3 =	0.013821				
r =	1.833623				
r21 =	1.296649				
r32 =	1.414125				
Theta 3 =	0.623				
Theta 2 =	0.6241				
Theta 1 =	0.6326				
e32 =	0.0011				
e21 =	0.0085				
q(p) =	-1.0305				
p =	11.83778				
s=	0.129051				
Theta ext21 =	0.633012				
Theta ext32 =	0.624119				

Orifice Beta = 0.65 Numerical Error

Density	999.7		**Approximate**		
Viscosity	0.001308		Relative Error $_{12}$=	0.190627	%
Velocity	2.788453		**Relative Error $_{23}$=**	**1.082286**	**%**
Grid # 1			**Extrapolated**		
Count =	70		Relative Error $_{12}$=	0.074294	%
Volume (m^3) =	0.04089	m^3	Relative Error $_{23}$=	0.215654	%
Cells =	158426				
h1 =	0.006367		**Grid Convergence Index**		
			GCI fine $_{12}$ =	0.005377	%
Grid # 2			GCI fine $_{23}$=	0.006259	%
Count =	50				
Volume =	0.04081	m^3	**Maximum Error =**	**1.10**	**%**
Cells =	60151				
h2 =	0.008787				
Grid # 3					
Count =	30				
Volume =	0.04051	m^3			
Cells =	15270				
h3 =	0.013844				
r =	2.17424				
r21 =	1.380097				
r32 =	1.575425				
Theta 3 =	0.6215				
Theta 2 =	0.6283				
Theta 1 =	0.6295				
e32 =	0.0068				
e21 =	0.0012				
q(p) =	-0.46373				
p =	3.944905				
s=	-0.5782				
Theta ext21 =	0.629968				
Theta ext32 =	0.629658				

Orifice Beta = 0.60 Numerical Error

Density	999.7	
Viscosity	0.001308	
Velocity	2.119029	
	Grid # 1	
Count =	60	
Volume (m^3) =	0.08153	m^3
Cells =	78296	
h1 =	0.010136	
	Grid # 2	
Count =	50	
Volume =	0.08142	m^3
Cells =	55500	
h2 =	0.011363	
	Grid # 3	
Count =	40	
Volume =	0.081238	m^3
Cells =	31327	
h3 =	0.013739	
r =	1.355458	
r21 =	1.121036	
r32 =	1.209112	
Theta 3 =	0.6101	
Theta 2 =	0.6098	
Theta 1 =	0.609	
e32 =	0.0003	
e21 =	0.0008	
q(p) =	-1.97001	
p =	25.82712	
s=	0.366273	
Theta ext21 =	0.608956	
Theta ext32 =	0.609798	

Approximate

Relative Error $_{12}$=	**0.131363**	**%**
Relative Error $_{23}$=	0.049196	%

Extrapolated

Relative Error $_{12}$=	0.007249	%
Relative Error $_{23}$=	0.000368	%

Grid Convergence Index

GCI fine $_{12}$ =	0.057272	%
GCI fine $_{23}$=	0.007263	%
Maximum Error =	**0.20**	**%**

Orifice Beta = 0.50 Numerical Error

Density	999.7		**Approximate**		
Viscosity	0.001308		Relative Error $_{12}$=	0.224863	%
Velocity	2.788453		**Relative Error $_{23}$=**	**0.849359**	**%**
Grid # 1			**Extrapolated**		
Count =	60		Relative Error $_{12}$=	0.113788	%
Volume (m^3) =	0.03802	m^3	Relative Error $_{23}$=	0.287239	%
Cells =	93916				
h1 =	0.007398				
			GCI fine $_{12}$ =	0.0118	%
Grid # 2			GCI fine $_{23}$=	0.018992	%
Count =	45				
Volume =	0.03795	m^3	**Maximum Error =**	**0.90**	**%**
Cells =	41539				
h2 =	0.009704				
Grid # 3					
Count =	30				
Volume =	0.03769	m^3			
Cells =	14814				
h3 =	0.013652				
r =	1.845402				
r21 =	1.311676				
r32 =	1.406904				
Theta 3 =	0.6187				
Theta 2 =	0.624				
Theta 1 =	0.6226				
e32 =	0.0053				
e21 =	0.0014				
q(p) =	-0.23984				
p =	4.02274				
s=	-0.6005				
Theta ext21 =	0.621892				
Theta ext32 =	0.625798				

V-Cone Beta = 0.6611 Numerical Error

Density	999.7	
Viscosity	0.001308	
Velocity	1.400577	
Count =	30	
Volume =	0.05188	m^3
Cells =	90177	
h3 =	0.008317	
Count =	45	
Volume =	0.05193	m^3
Cells =	147303	
h2 =	0.007065	
Count =	60	
Volume (m^3) =	0.05196	m^3
Cells =	490265	
h1 =	0.004733	
r =	1.757463	
r21 =	1.492752	
r32 =	1.177331	
Theta 3 =	0.8038	
Theta 2 =	0.7972	
Theta 1 =	0.7981	
e32 =	0.0066	
e21 =	0.0009	
q(p) =	3.160418	
p =	12.86213	
s=	0.867497	
Theta ext21 =	0.798105	
Theta ext32 =	0.796279	

Approximate

Relative Error $_{12}$=	0.112768	%
Relative Error $_{23}$=	**0.827898**	**%**

Extrapolated

Relative Error $_{12}$=	0.000656	%
Relative Error $_{23}$=	0.115697	%

Grid Convergence Index

GCI fine $_{12}$ =	0.115471	%
GCI fine $_{23}$=	0.144454	%
Maximum Error =	**0.90**	**%**

V-Cone Beta = 0.6995 Numerical Error

Density	999.7		**Approximate**		
Viscosity	0.001308		Relative Error $_{12}$=	0.736395	%
Velocity	1.668341		Relative Error $_{23}$=	0.440086	%
Count =	20		**Extrapolated**		
Volume =	0.1672	m^3	Relative Error $_{12}$=	1.272741	%
Cells =	82059		Relative Error $_{23}$=	0.86822	%
h3 =	0.012678				
			Grid Convergence Index		
Count =	28		**GCI fine $_{12}$ =**	**1.611436**	**%**
Volume =	0.1679	m^3	GCI fine $_{23}$=	1.094781	%
Cells =	152156				
h2 =	0.010334		**Maximum Error =**	**1.70**	**%**
Count =	35				
Volume (m^3) =	0.1683	m^3			
Cells =	301259				
h1 =	0.008236				
r =	1.539289				
r21 =	1.254695				
r32 =	1.226823				
Theta 3 =	0.7918				
Theta 2 =	0.7953				
Theta 1 =	0.8012				
e32 =	0.0035				
e21 =	0.0059				
q(p) =	0.070333				
p =	1.991499				
s=	0.559034				
Theta ext21 =	0.811529				
Theta ext32 =	0.802265				

V-Cone Beta = 0.8203 Numerical Error

Density	999.7	
Viscosity	0.001308	
Velocity	1.399	
Count =	20	
Volume =	0.2348	m^3
Cells =	121563	
h3 =	0.012454	
Count =	29	
Volume =	0.2351	m^3
Cells =	175424	
h2 =	0.01103	
Count =	36	
Volume (m^3) =	0.2808	m^3
Cells =	345269	
h1 =	0.009335	
r =	1.33419	
r21 =	1.18115	
r32 =	1.12956	
Theta 3 =	0.7304	
Theta 2 =	0.7338	
Theta 1 =	0.7388	
e32 =	0.0034	
e21 =	0.005	
q(p) =	0.135863	
p =	1.500355	
s=	0.628793	
Theta ext21 =	0.75642	
Theta ext32 =	0.750752	

Approximate

Relative Error $_{12}$=	0.6767	%
Relative Error $_{23}$=	0.4633	%

Extrapolated

Relative Error $_{12}$=	**2.3293**	**%**
Relative Error $_{23}$=	2.2580	%

Grid Convergence Index

GCI fine $_{12}$ =	2.1517	%
GCI fine $_{23}$=	2.1092	%
Maximum Error =	**2.40**	**%**

6 Inch Wedge Beta = 0.5023 Numerical Error

Density	999.7	
Viscosity	0.001308	
Velocity	2.788	
Count =	24	
Volume =	0.03945	m^3
Cells =	39845	
h3 =	0.009967	
Count =	30	
Volume =	0.03953	m^3
Cells =	64304	
h2 =	0.008503	
Count =	35	
Volume (m^3) =	0.03958	m^3
Cells =	93490	
h1 =	0.007509	
r =	1.327353	
r21 =	1.13238	
r32 =	1.172179	
Theta 3 =	0.7374	
Theta 2 =	0.7297	
Theta 1 =	0.7272	
e32 =	0.0077	
e21 =	0.0025	
q(p) =	-0.24904	
p =	7.045376	
s=	0.061554	
Theta ext21 =	0.725416	
Theta ext32 =	0.725967	

Approximate

Relative Error $_{12}$=	0.343784	%
Relative Error $_{23}$=	**1.055228**	**%**

Extrapolated

Relative Error $_{12}$=	0.245986	%
Relative Error $_{23}$=	0.514233	%

Grid Convergence Index

GCI fine $_{12}$ =	0.306727	%
GCI fine $_{23}$=	0.639503	%
Maximum Error =	**1.10**	**%**

8 Inch Wedge Beta = 0.5023 Numerical Error

Density	999.7	
Viscosity	0.001308	
Velocity	2.119	
Count =	24	
Volume =	0.08643	m^3
Cells =	37672	
h3 =	0.01319	
Count =	29	
Volume =	0.08662	m^3
Cells =	57140	
h2 =	0.011488	
Count =	36	
Volume (m^3) =	0.08675	m^3
Cells =	134453	
h1 =	0.008641	
r =	1.526325	
r21 =	1.329408	
r32 =	1.526325	
Theta 3 =	0.7401	
Theta 2 =	0.7318	
Theta 1 =	0.7276	
e32 =	0.0083	
e21 =	0.0042	
q(p) =	-0.39338	
p =	1.010754	
s=	0.918947	
Theta ext21 =	0.715006	
Theta ext32 =	0.716236	

Approximate

Relative Error $_{12}$=	0.57724	%
Relative Error $_{23}$=	1.13419	%

Extrapolated

Relative Error $_{12}$=	1.761421	%
Relative Error $_{23}$=	**2.173027**	**%**

Grid Convergence Index

GCI fine $_{12}$ =	0.112147	%
GCI fine $_{23}$=	0.075926	%
Maximum Error =	**2.20**	**%**

Wedge Beta = 0.611 Numerical Error

Density	999.7	
Viscosity	0.001308	
Velocity	2.119	
Count =	27	
Volume =	0.08765	m^3
Cells =	84869	
h3 =	0.010109	
Count =	30	
Volume =	0.08769	m^3
Cells =	121245	
h2 =	0.008977	
Count =	33	
Volume (m^3) =	0.08768	m^3
Cells =	345485	
h1 =	0.006332	
r =	1.596523	
r21 =	1.417762	
r32 =	1.126086	
Theta 3 =	0.7016	
Theta 2 =	0.7056	
Theta 1 =	0.7075	
e32 =	0.004	
e21 =	0.0019	
q(p) =	2.370625	
p =	8.923647	
s=	0.86054	
Theta ext21 =	0.707588	
Theta ext32 =	0.707722	

Approximate

Relative Error $_{12}$=	0.268551	%
Relative Error $_{23}$=	**0.566893**	**%**

Extrapolated

Relative Error $_{12}$=	0.012469	%
Relative Error $_{23}$=	0.299773	%

Grid Convergence Index

GCI fine $_{12}$ =	0.031379	%
GCI fine $_{23}$=	0.541522	%
Maximum Error =	**0.60**	**%**